Radboud University Nijmegen

Faculty of Science

New Physics or Awkward Reflection

An Investigation of Anomalous ANITA Measurements Using Simulated Propagation of Radio Signals From Air Showers

Thesis BSc Physics and Astronomy

Author:
Colin Saba

Supervisor:
dr. H. Schoorlemmer

Second reader:
dr. S. Westhoff

February 2023

Abstract

The Antarctic Impulsive Transient Antenna (ANITA) is an experiment designed to measure Askaryan radiation from neutrino interactions in ice. During its flight it has encountered radio signals from ultra high energy cosmic ray induced air showers. Some of these radio signals' polarity remain uninverted after reflection off the Antarctic ice sheet. Different ice geometries, some of which rely on total internal reflection, are looked at to find an explanation for these anomalous measurements. It is shown that a construction can be made that results in a non-inverted radio signal, however, these are restricted by relatively big arrival angles. Introducing more inclinations in the construction leads to a situation which also works for the smaller arrival angles seen by ANITA.

Contents

1 Introduction

Every second the Earth is bombarded with charged particles from outer space. These particles, cosmic rays, have varying energy, some even up to 10^{20} Ev[1]. Cosmic rays collide with particles in the atmosphere and create cascades of charged particles, air showers. The charged particles in air showers interact with Earth's magnetic field, which results in radio signals that can be measured.

A description of these radio signals is possible, since we have Maxwell's equations, which have been well established since 1865. A few radio signals from air showers measured above Antarctica do not seem to care about these equations. Showing no phase shift upon reflection off the Antarctic ice sheet, these signals have no proper explanation.

In this thesis the experiment responsible for these measurements will be looked at and a simulation for radio signals from air showers will be build to investigate this behaviour and find a possible solution to this problem.

2 Ultra High Energy Cosmic Rays and Air Showers

Cosmic rays are charged particles travelling near light speed through space with energies up to 10^{20}eV [2]. Cosmic rays were first discovered in August 1912 by Victor Hess. While making a balloon flight he measured an increase in ionizing radiation [1]. From this he concluded that charged particles must penetrate the atmosphere. Since the discovery, cosmic rays have played an important role in particle physics. It has lead to the discovery of new particles such as pions and muons [3]. The cosmic rays mainly consist of hydrogen nuclei ($\sim 90\%$). Cosmic rays traverse the universe and are directed by the magnetic fields they encounter. On Earth, cosmic rays are observed isotropically in the atmosphere, increasing the difficulty of determining their origin. The flux of these cosmic rays fall of with energy. This fall off is proportional to $E^{-\gamma}$, where $\gamma \sim 2.7$ [4]. This makes higher energy cosmic rays increasingly harder to observe. For energies in the order of 10^{18}eV and higher we speak of ultra high energy cosmic rays (UHECRs).

Instead of observing cosmic rays directly, the shower of secondary particles they create can be observed. As cosmic rays enter Earth's atmosphere they interact with particles in the air. Collisions create new particles with high enough energy to create new particles in a next collision. This process repeats itself until there are particles left with insufficient energy to create new particles in collisions. This cascade of particles created in collisions and the decay of existing particles are extensive air showers.

These extensive air showers emit radio signals with frequencies in the MHz domain, that can be measured. There are two mechanisms responsible for this emission of radio signals. The first, and dominant mechanism, is the geomagnetic mechanism [5]. As charged particles in the air shower travel through the geomagnetic field, they experience a force

$$\mathbf{F} = q\mathbf{v} \times \mathbf{B}, \tag{2.1}$$

which is just the Lorentz force. The acceleration of the charged particles results in linearly polarized radio emission, with polarization along the $-\mathbf{v} \times \mathbf{B}$ direction. The second mechanism is the Askaryan mechanism. As the air shower forms, the particles knock electrons away from their atoms. These electrons travel along the shower front while leaving behind positively charged ions. This results in a effective current along the shower axis resulting in radially polarized radio signals. The measured radio signals are superpositions of these two mechanisms. The latter mechanism will not be used in the simulations build later in this work.

3 Antarctic Impulsive Transient Antenna

In the austral summer of 2006 the Antarctic Impulsive Transient Antenna (ANITA) made its first flight, see figure 3.1. Above the continent of Antarctica, ANITA looks over 1.5 M

(a) ANITA-I, photo adapted from [6]

(b) ANITA-III making its ascend for its flight (Photo by Harm Schoorlemmer).

Figure 3.1: The Antarctic Impulsive Transient Antenna (left) and its flight (right).

km^2 of the Antarctic ice sheet. The antenna is flying over the continent at altitudes between 35-37km. ANITA registers all radio pulses of nanosecond duration over a frequency band of 200-1200MHz [7]. Initially the goal of the experiment was to measure Askaryan radiation from neutrino interactions in ice, which it, unfortunately, has never been able to do. What did happen, however, was the completely unanticipated measurement of radio signals from UHECRs induced air showers.

3.1 ANITA Measurements

For the measurement of radio signals from UHECRs induced air showers the situation is as shown schematically in figure 3.2.

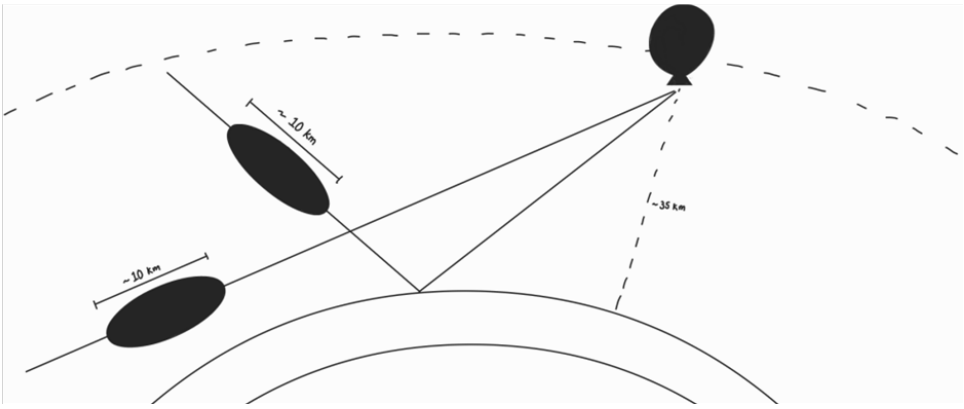

Figure 3.2: The geometry for measurements of radio signals from air showers by ANITA. The black ovals represent air showers and the balloon represents ANITA.

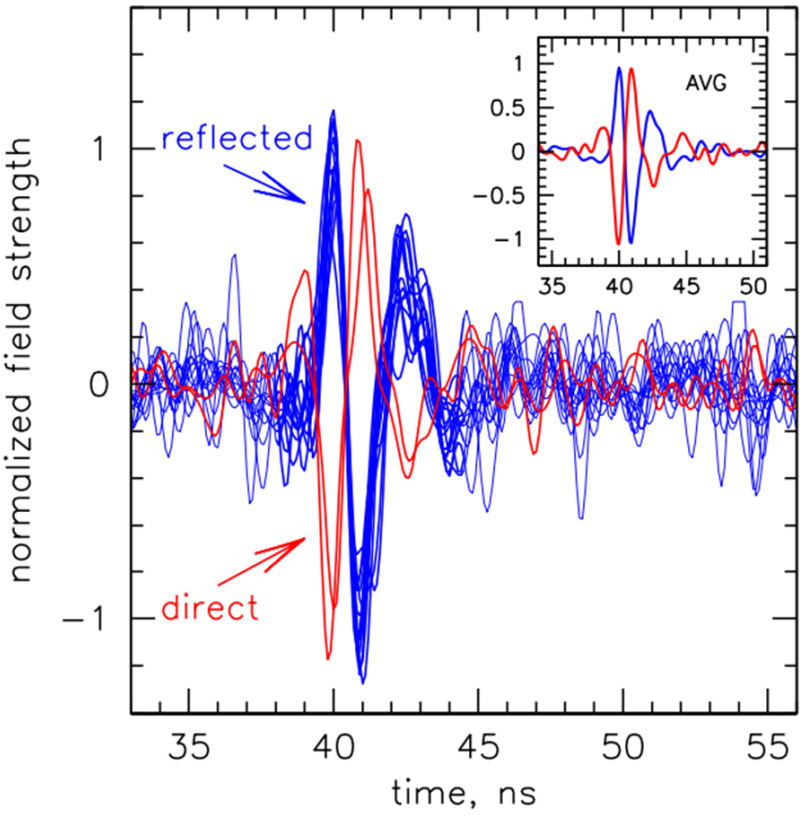

Figure 3.3: The measurements from ANITA-I. In red are the direct measurements and in blue the reflected measurements. Figure adapted from [7].

Here we see two cases that can happen. Either ANITA measures a signal directly, because the radio signal from the air shower comes over the horizon. Or, ANITA measures a signal after it has been reflected off the ice sheet. In the latter case the polarity of the signal is inverted, as demanded by Maxwell's equations. This is discussed in section 4.2.1. For the ANITA-I flight there are 16 measurements, the results of which are shown in figure 3.3. Two of these measurements where measured directly as they came over the horizon to ANITA, fourteen of them were measured after reflection off ice. Here we see exactly what we would expect, the reflected signals are inverted with respect to the direct measurements.

3.2 Anomalous Measurements During ANITA-I and ANITA-III

In the third flight of ANITA from the 18$^{\text{th}}$ of December, 2014 through the 8$^{\text{th}}$ of January 2015, again measurements such as the ones during ANITA-I were made. This time, however, there were three direct observations, from which only two where measured above the horizon. The third direct measurement could be traced back to the ice, suggesting a reflection. In this last case we would expect a polarity inversion, which was not the case [8], see figure 3.4. Here we see four events, two of which came over the horizon. Event 15717147 marks our anomalous measurement. Event 68298837 is characterized by a similar angle as the anomalous signal[i]. In the first flight such a measurement was also made, but it could not be ruled out that it was due to human activity. The ANITA-I and ANITA-III measurements mark the starting point of the problem of the anomalous ANITA measurements. When looking at the shape of the measured signal, it is very similar to those of the reflected signals, all of which are in good agreement

[i]The angles are given with respect to the horizontal direction of the antenna.

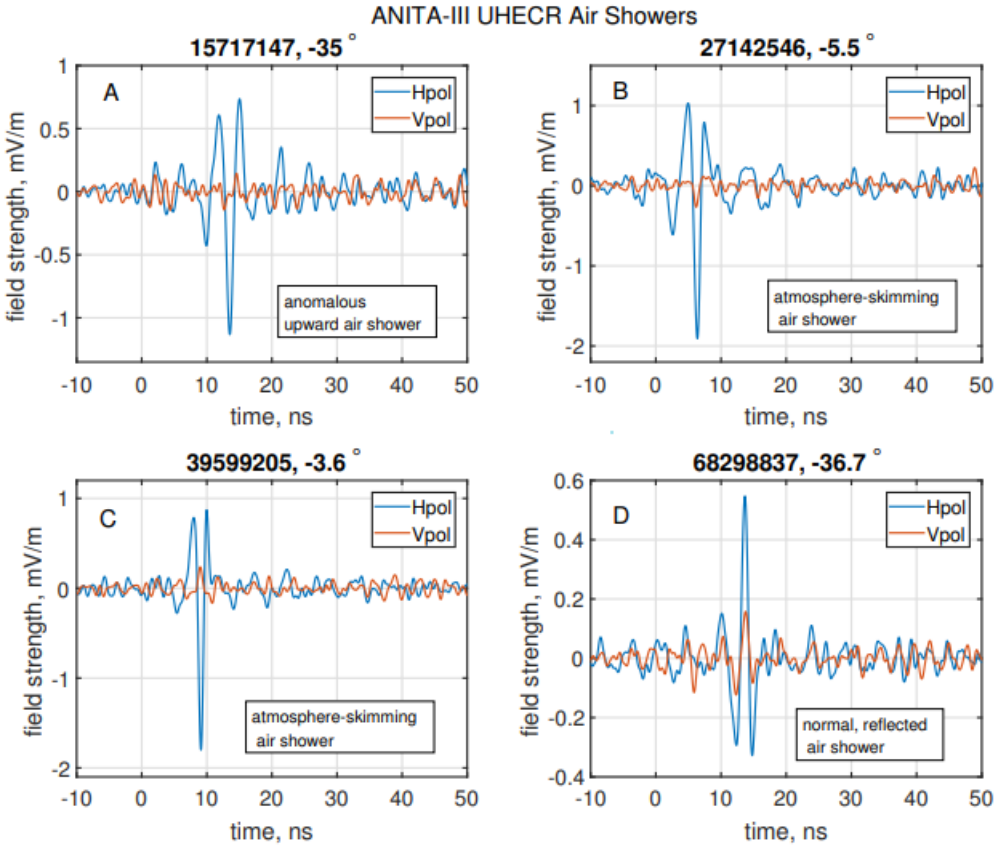

Figure 3.4: The field strengths of the two polarizations of the electric field for three non-inverted signals measured during ANITA-III (A,B and C) and a inverted signal (D). B and C are direct measurements that came over the horizon, A is the anomalous measurement. Figure adapted from [8]

with the the template for such signals [8], see figure 3.5. This suggest a common origin for all these radio signals.

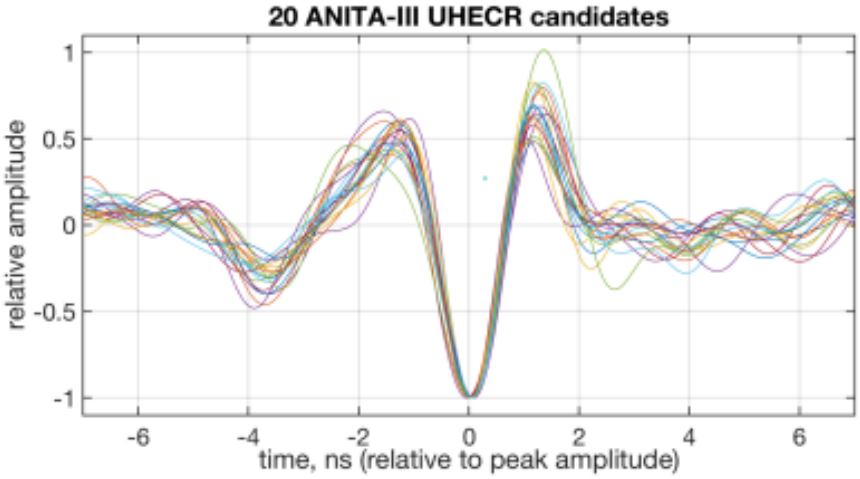

Figure 3.5: The 20 ANITA-III measurements, with the inverted measurements now uninverted. The similarity of these signals with each other and the expectations suggest a common origin: UHECRs. Figure adapted from [8].

3.3 ANITA-IV and More Anomalous Measurements

In 2016 the fourth flight of ANITA took place. During this flight 29 cosmic ray like events were measured. Many of which were measurements such as the inverted measurements of previous flights. Four of these measurements showed no inversion of polarity, just as in the ANITA-I and ANITA-III flights. This time, however, these anomalous measurements were characterized by big zenith angles, arriving near horizontally at ANITA [9].

3.4 New Physics as an Explanation for Anomalous ANITA Measurements

Finding an explanation for the anomalous ANITA measurements have been the goal for some papers, see [8, 10]. Both of these papers have explanations beyond the standard model. P.W. Gorham et al. [8] discuss the possibility of the decay of an upward travelling τ-lepton, produced by a ν_τ. However, as explained in this paper by P.W. Gorham et al., the zenith angle of the anomalous events create tension with the standard model. It is very improbable for a ν_τ to travel the necessary distance through the Earth, as the cross section for an interaction is too big at the energies relevant here. ν_τ as an explanation for the anomalous ANITA measurements would imply that the cross section for neutrino interactions should be smaller at these energies, or an increase in flux of neutrinos [8].

Other explanations for the ANITA measurements exist, like a supersymmetric approach, see [10].

The focus of this thesis will be on the propagation of the radio signals emitted by air showers. In the propagation an explanation will be sought for the anomalous ANITA measurements.

4 Basic Phenomena in Optics

In order to be able to simulate CR-like events, like event 15717147 from the ANITA-III flight, some important concepts from optics need to be implemented. In this section the most important phenomena from optics that will play a role in the simulation will be discussed.

4.1 The Electric Field

The electric field in a isotropic, homogeneous and nonconducting material is given by [11]

$$\nabla^2 \mathbf{E} - \epsilon_0 \mu_0 \frac{\partial^2 \mathbf{E}}{\partial t^2} = \mu_0 \frac{\partial^2 \mathbf{P}}{\partial t^2} \tag{4.1}$$

For the case of plane wave solutions $\mathbf{E} = \mathbf{E}_0 e^{i\mathbf{k}\cdot\mathbf{r}-\omega t}$ and no absorption, we get for the polarization [11, 12]

$$\mathbf{P} = \epsilon_0 \left(n^2 - 1\right) \mathbf{E}_0 e^{i\mathbf{k}\cdot\mathbf{r}-\omega t}. \tag{4.2}$$

Taking these plane waves we can construct any arbitrary waveform and simulate their behaviour during propagation. In our case we will work with a delta function signal, which is just a superposition of all plane waves

$$\mathbf{E}(\mathbf{r}, t) \propto \mathbf{E}_0 \int_{-\infty}^{\infty} e^{i(\mathbf{k}\cdot\mathbf{r}-\omega t)} \mathrm{d}\omega. \tag{4.3}$$

Using the dispersion relation $\mathbf{k} = \frac{n\omega}{c}\hat{\mathbf{k}}$ [11] yields

$$\mathbf{E}(\mathbf{r}, t) \propto \frac{\mathbf{E}_0}{2\pi} \delta\left(t - \frac{n}{c}\hat{\mathbf{k}} \cdot \mathbf{r}\right). \tag{4.4}$$

In equation 4.4 the second term in the delta function gives a time delay due to propagation. Since n will be assumed to be independent of frequency, we will have no deformation of our signal, an explicit calculation for this will be given later on.

4.2 Reflection and Refraction

With an explicit electric field given, the first problem is that of an electromagnetic wave incident on the interface between two materials. As will be discussed in section 5.1, the atmosphere, through which we will let a signal propagate, will be assumed to consist of many thin layers of constant refractive index. At each of the interfaces the problem of reflection and refraction needs to be solved. At a single interface the situation is shown in figure 4.1. Here the subscript i, r and t denote the incident, reflected and transmitted fields, respectively. From figure 4.1 we can write the electric fields as, see also [11],

$$\begin{aligned}
\mathbf{E}_i &= \left(E_i^{(p)} \left(\hat{\mathbf{x}} \cos\theta_i + \hat{\mathbf{z}} \sin\theta_i\right) + \hat{\mathbf{y}} E_i^{(s)}\right) e^{i(\mathbf{k}_i\cdot\mathbf{r}-\omega_i t)} \\
\mathbf{E}_r &= \left(E_r^{(p)} \left(\hat{\mathbf{x}} \cos\theta_r - \hat{\mathbf{z}} \sin\theta_r\right) + \hat{\mathbf{y}} E_r^{(s)}\right) e^{i(\mathbf{k}_r\cdot\mathbf{r}-\omega_r t)} \\
\mathbf{E}_t &= \left(E_t^{(p)} \left(\hat{\mathbf{x}} \cos\theta_t + \hat{\mathbf{z}} \sin\theta_t\right) + \hat{\mathbf{y}} E_t^{(s)}\right) e^{i(\mathbf{k}_t\cdot\mathbf{r}-\omega_t t)}.
\end{aligned} \tag{4.5}$$

Maxwell's equations give us boundary conditions on the electric and magnetic fields. The components parallel to the interface of both the electric and magnetic field should be equal on both sides of a boundary [11]. This results in the following conditions

$$\omega_i = \omega_r = \omega_t = \omega \tag{4.6}$$

and Snell's law

$$n_i \sin\theta_i = n_i \sin\theta_r = n_t \sin\theta_t, \tag{4.7}$$

which will be used extensively. Using the said boundary conditions the amplitudes of both polarizations of the electric field can be related via Fresnel coefficients.

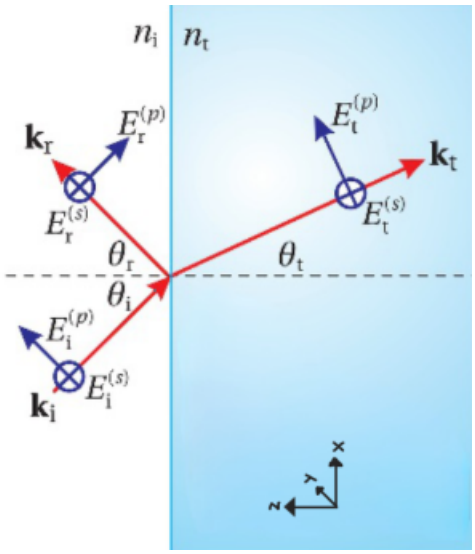

Figure 4.1: The situation for reflection and refraction at a single interface. p and s denote the electric field component parallel and normal to the plane of incidence, respectively. i, r and t are the incident, reflected and transmitted electric fields, respectively. Figure adapted from [11] and is slightly modified.

4.2.1 Fresnel Coefficients

The Fresnel coefficients are a set of four coefficients that relate the different electric field components across a boundary [11]. For reflection of the p and s polarizations we get equations 4.8 and 4.9.

$$r_s = \frac{E_r^{(s)}}{E_i^{(s)}} = \frac{n_i \cos\theta_i - n_t \cos\theta_t}{n_i \cos\theta_i + n_t \cos\theta_t} \tag{4.8}$$

$$r_p = \frac{E_r^{(p)}}{E_i^{(p)}} = \frac{n_i \cos\theta_t - n_t \cos\theta_i}{n_i \cos\theta_t + n_t \cos\theta_i} \tag{4.9}$$

Obviously, these equations will play an important role for reflection of ice. The values of r_p and r_s, as a function of the angle of incidence, for an air to ice interface, are plotted in figure 4.2. These coefficients will determine the phase shift of the different components of the electric field upon reflection. It is therefore that these coefficients will play an important role in this work, to find an apparent reflection with no phase shift.

For the transmission of the two polarizations we get equations 4.10 and 4.11.

$$t_s = \frac{E_t^{(s)}}{E_i^{(s)}} = \frac{2n_i \cos\theta_i}{n_i \cos\theta_i + n_t \cos\theta_t} \tag{4.10}$$

$$t_p = \frac{E_t^{(p)}}{E_i^{(p)}} = \frac{2n_i \cos\theta_i}{n_i \cos\theta_t + n_t \cos\theta_i} \tag{4.11}$$

The values of these coefficients are also shown in figure 4.2. These will also play a role in the possible transmission through ice. These coefficients are for an air-ice interface always positive and therefore will not introduce a phase shift of the signal. They will, however, tell us about the amplitude of the signal after transmission. The transmission and reflection coefficients will be ignored for propagation through the air. As will be discussed later, these have little significance on the amplitudes for the considered situations of propagation through air.

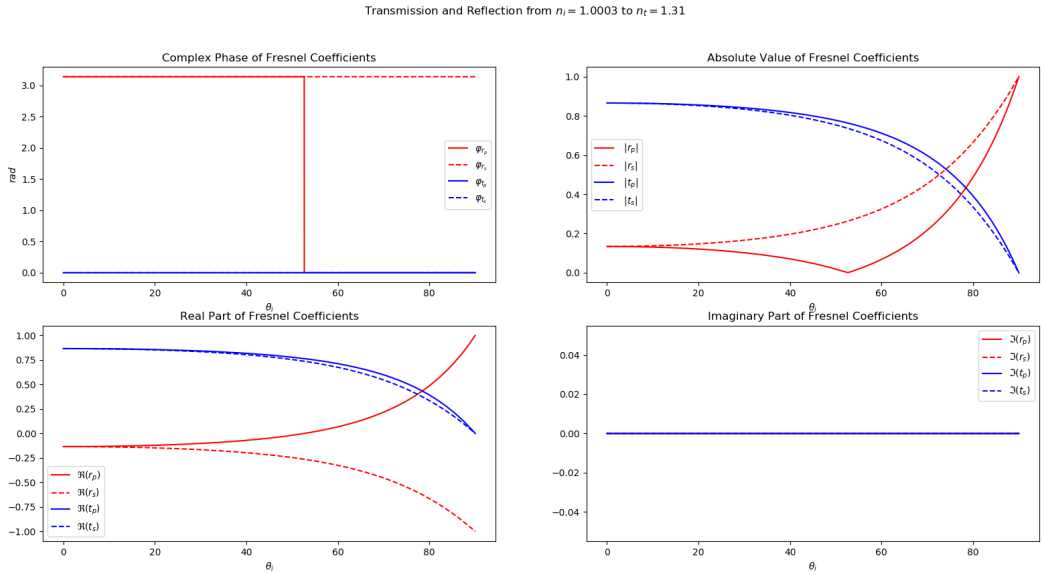

Figure 4.2: The phase and values of the Fresnel coefficients for transmission and reflection from air to ice.

One thing worth mentioning is what we see for r_p. As can be seen in figure 4.2, r_p intersects the horizontal axis. This means that there is an angle for which the p polarization is not reflected. This angle is denoted by θ_B, the Brewster angle. This occurs, because for $\theta_i = \theta_B$ the reflected and transmitted fields are orthogonal. A reflection of the p polarization in this case would require the dipoles in the material to emit along their axis, which cannot happen. The Brewster angle is given by [11]

$$\theta_B = \arctan \frac{n_t}{n_i}. \tag{4.12}$$

4.3 Total Internal Reflection and Mirages

From equations 4.8-4.11 the fraction of power that is reflected from and that is transmitted through a surface can be found. The transmittance and reflectance are defined as [11]

$$\begin{aligned} R_s &= |r_s|^2; \\ R_p &= |r_p|^2; \\ T_s &= 1 - R_s; \\ T_p &= 1 - R_p. \end{aligned} \tag{4.13}$$

The reflectance and transmittance for an air-ice interface and an ice-air interface are plotted in figure 4.3. Here we can see that in the case of an ice to air interface, there is a point at which all power of the incident wave is reflected for angles greater than the cutoff: total internal reflection (TIR). This can only happen for propagation from a medium with refractive index n_i to a medium with refractive index n_t when $n_i > n_t$. TIR occurs if the transmitted angle, determined using Snell's law, equation 4.7, becomes imaginary. The condition for total internal reflection is, see also [12],

$$\theta \geq \theta_c \equiv \sin^{-1} \frac{n_t}{n_i}. \tag{4.14}$$

Physically, θ_c corresponds to the angle for which the angle of transmitance is 90°.

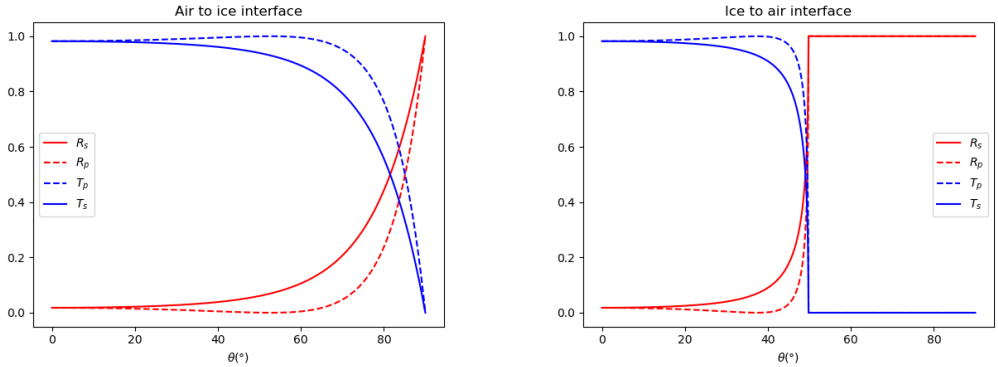

(a) (b)

Figure 4.3: Reflectance and transmittance for an air to ice interface (a) and an ice to air interface (b).

4.3.1 Mirages

The refractive index of a gas is proportional to the density of that gas, this is given by the Gladstone-Dale relation [13],

$$(n-1) \propto \rho. \tag{4.15}$$

Using the ideal gas law we know that $\rho \propto \frac{P}{T}$. From this it follows that, see [14],

$$(n-1) \propto \frac{1}{T}. \tag{4.16}$$

Equation 4.16 gives rise to two types of mirages. On hot days the ground is heated up, which in turn warms the air above it. According to equation 4.16 this gives rise to a lower index of refraction. Looking at the air as infinitesimally thin layers of constant refractive index, total internal reflection can occur for big enough angles, see the right panel of figure 4.4. This give rise to an apparent different location of an object, if looked at in the visible light spectrum, this is called an inferior mirage.

In the polar regions the air close to the ground is cooled, which in turn cooles down the lower layers in the atmosphere. Using equation 4.16, this results in a greater refractive index. Light is bend more downwards in these regions, this is a superior mirage, see the left panel of figure 4.4.

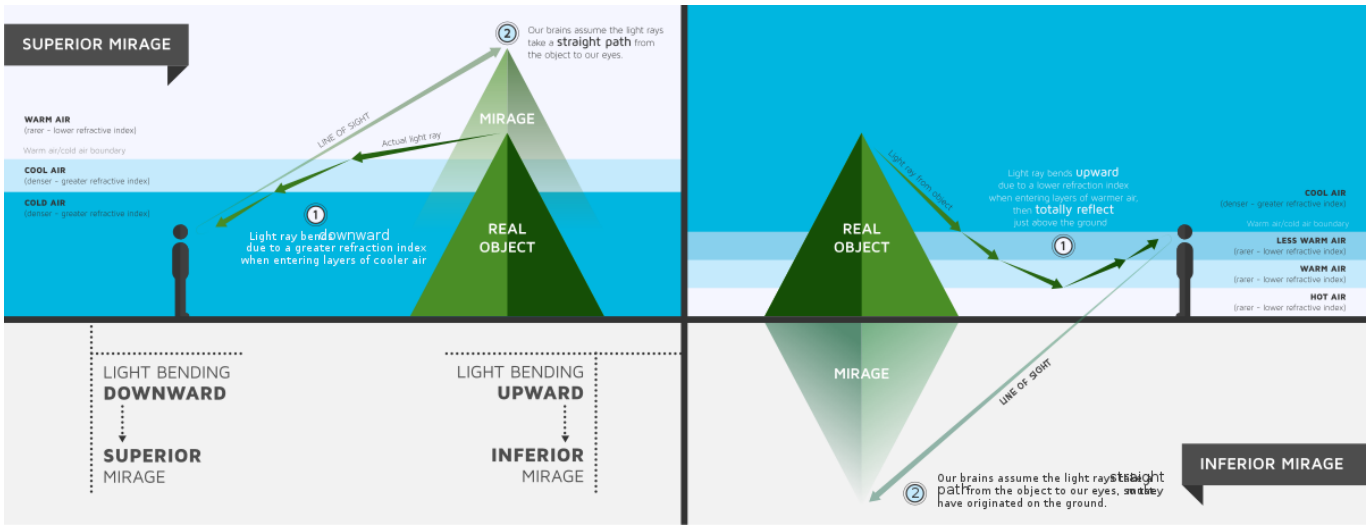

Figure 4.4: Inferior (right) and superior (left) mirages [15].

4.4 Coherence

The last important concept we need to look at is coherence. When looking at radio signals coming from air showers, they come from different places in the air shower. The time it takes for them to arrive at an antenna will determine if they can interfere constructively, and are therefore coherent. An example is given in figure 4.5. Here we have used Gaussians for the radio signal. In the left panel we see two signals which have such a time difference that they do not interfere constructively, they are incoherent. In the right panel the time differences are small enough such that the signals are coherent and interfere constructively. It is this last scenario we are after in the simulation.

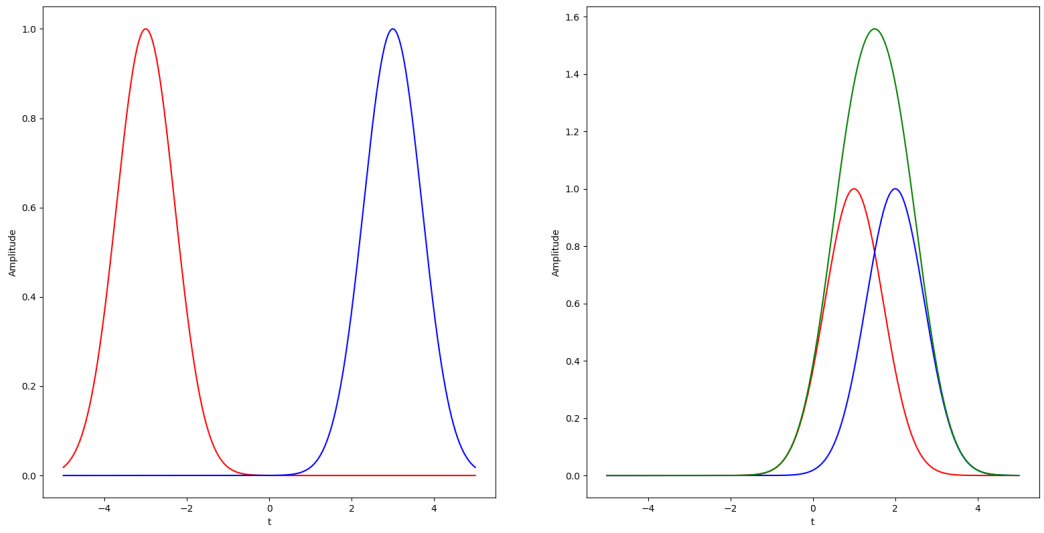

Figure 4.5: An example of coherence using Gaussians. In the left panel the signals are incoherent. In the right panel they are coherent. The green function is the sum of the individual signals.

As will be discussed later we will assume the radio signals to originate all from somewhere along the shower axis. From this we can determine where we would expect our signal to be

coherent. For this we will assume the paths of the signals to be parallel. As we will see later the path is way longer than the spacing between pulses, it is therefore that this assumption is reasonable. For the last and first signal to be coherent (or any two signals from the air shower), we get a situation as in figure 4.6.

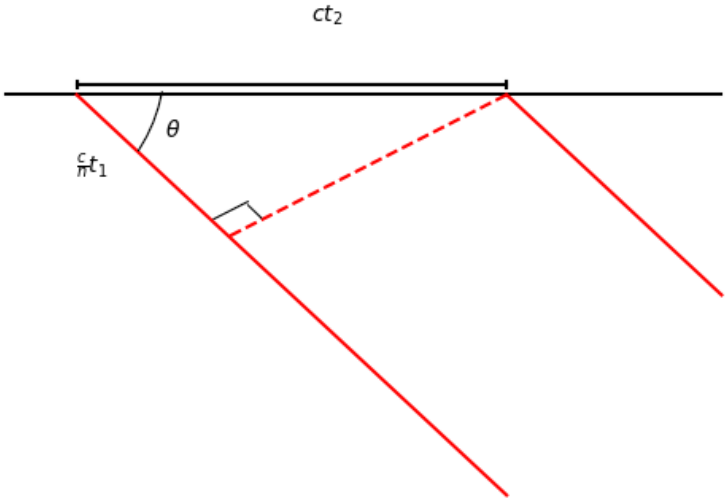

Figure 4.6: Two signals emitted at an angle θ from the shower axis.

If we want the two signals to arrive at the same time we must demand that $t_1 = t_2$. For the angle θ this implies

$$\cos\theta = \frac{1}{n}, \tag{4.17}$$

which is the Cherenkov angle. It is this angle for which we expect the signal measured from the air shower to be most coherent. For angles close to the Cherenkov angle the signal will still, for the most part, be coherent. This gives rise to the Cherenkov cone. For air the refractive index is very close to 1. From this we will expect our signal to be most coherent for angles θ close to $0°$. Later we will show that this is exactly what is found in the simulation.

5 Simulating Radio Signals From Air Showers

The goal is to simulate radio signals from air showers in the frequency regime ANITA is sensitive to, i.e. 200-1200 MHz [7]. To achieve this an air shower will be approximated as an emitter traveling at light speed through the atmosphere at some zenith angle with respect to the z axis. The paths that emitted radio signals follow are important, as this induces a shift in the arrival time of a signal at the location where it will be received.

5.1 The Atmosphere

To simulate a radio signal propagating through the atmosphere the refractive index of the atmosphere is needed. The refractive index can be approximated by a exponential function that only depends on the altitude z [16]

$$n\left(z\right) = 1 + \eta_0 e^{-\kappa z} \tag{5.1}$$

where $\eta_0 = 325 \cdot 10^{-6}$ and $\kappa = 0.0001218 m^{-1}$. By taking a function only dependent on the height, the curvature of the Earth is implicitly ignored. This assumption is deemed reasonable, for a discussion of this, see appendix A.

In this model the atmosphere will be discretized. This way it becomes a system of many layers of equal thickness d. The refractive index of each layer will be taken in the center of the layer and will be assumed to be constant across the thickness of the layer, giving a model as shown in figure 5.1.

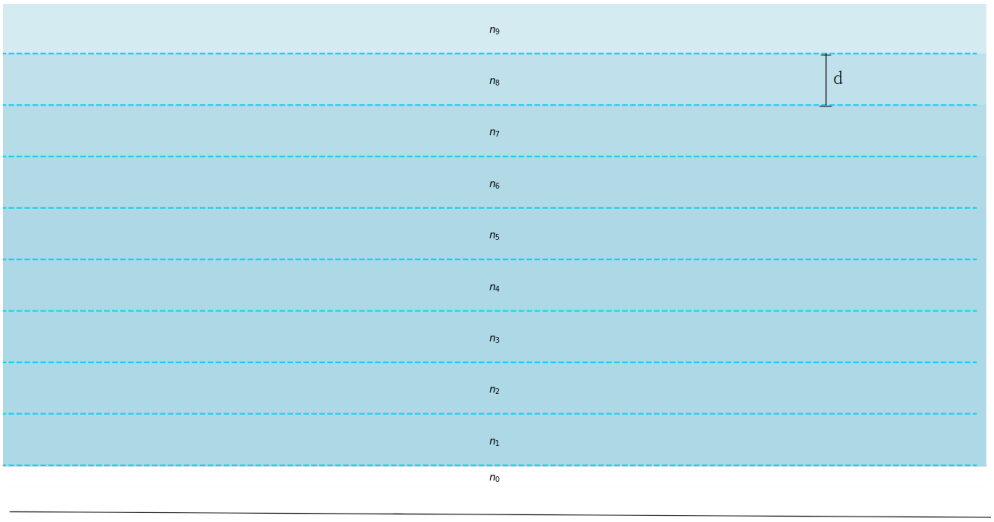

Figure 5.1: An atmosphere of many layers of thickness d and constant refractive index as given by equation 5.2.

For the refractive index of the i-th layer we have

$$n_i = 1 + \eta_0 e^{-\kappa\left(i+\frac{1}{2}\right)\cdot d}. \tag{5.2}$$

The layer $i = 0$ corresponds to the Antarctic ice sheet, the value of n_0 is taken to be 1.33 [7].

5.2 Propagation and Refraction

The next step is to let a signal propagate through this system of many layers. Determining the path a signal will take boils down to solving a refraction problem at each interface. Since air is

isotropic we only need two dimensions to describe the path, this is chosen to be the xz-plane. Let (x_0, z_0) denote the coordinates where the signal originates from. If $z_0 \mod d = 0$, the coordinate pair (x_0, z_0) is located at the $\lceil \frac{z_0}{d} \rceil$-th interface. Otherwise it is located in the $\lceil \frac{z_0}{d} \rceil$-th layer. To proceed in the latter case, the intersection of the signal's path and next interface needs to be located. This is a problem of simple geometry.

Let the signal originate in the i-th layer and denote the angle of incidence upon the interface with the $i-1$-th layer by θ_i. Then we can form a right triangle of sides $z_0 - \lfloor \frac{z_0}{d} \rfloor d$ and $x_1 - x_0$, see figure 5.2. From this follows (x_1, z_1):

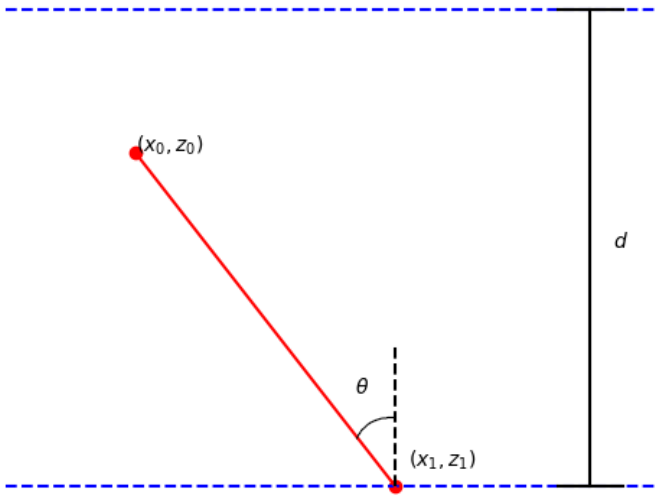

Figure 5.2: The geometry for the situation when (x_0, z_0) does not coincide with an interface.

$$(x_1, z_1) = \left(x_0 + \left(z_0 - \left\lfloor \frac{z_0}{d} \right\rfloor d \right) \cdot \tan\theta_i, \left\lfloor \frac{z_0}{d} \right\rfloor d \right). \tag{5.3}$$

For the coordinates of a point on the interface between arbitrary layers we can find a recurrence relation. The situation of refraction at single interface is shown in figure 5.3.

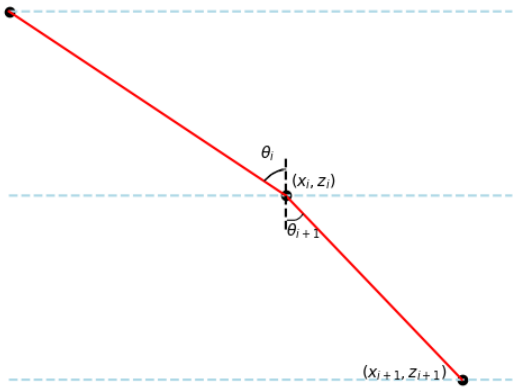

Figure 5.3: The situation for refraction upon entering a new layer in the atmosphere. θ_i is the angle of incidence and θ_{i+1} is the angle of refraction. These angles lead to propagation of the signal from (x_i, z_i) to (x_{i+1}, z_{i+1}).

Again forming a right triangle, this time with sides $z_i - z_{i+1} = d$ and $x_{i+1} - x_i$ we find

$$\tan\theta_{i+1} = \frac{x_{i+1} - x_i}{d}.$$

Using Snell's law, equation 4.7, this can be written as

$$x_{i+1} = x_i + \frac{d\frac{n_i}{n_t}\sin\theta_i}{\sqrt{1-\frac{n_i^2}{n_t^2}\sin^2\theta_i}} \tag{5.4}$$

where n_i and n_t are the refractive indices on the incident and transmitted side, respectively. Since Snell's law holds across each interface, equation 5.4 can be written solely in terms of the angle of incidence upon the first interface and the refractive index in the layer where the signal is emitted. Together with

$$z_{i+1} = z_i - d, \tag{5.5}$$

the whole path from emittance to the ice is determined. For the upward path after reflection equation 5.4 still holds. For the height we use

$$z_{i+1} = z_i + d. \tag{5.6}$$

Together with a reflection from the ice the whole path of the radio signal is fixed and can be simulated, see figure 5.4.

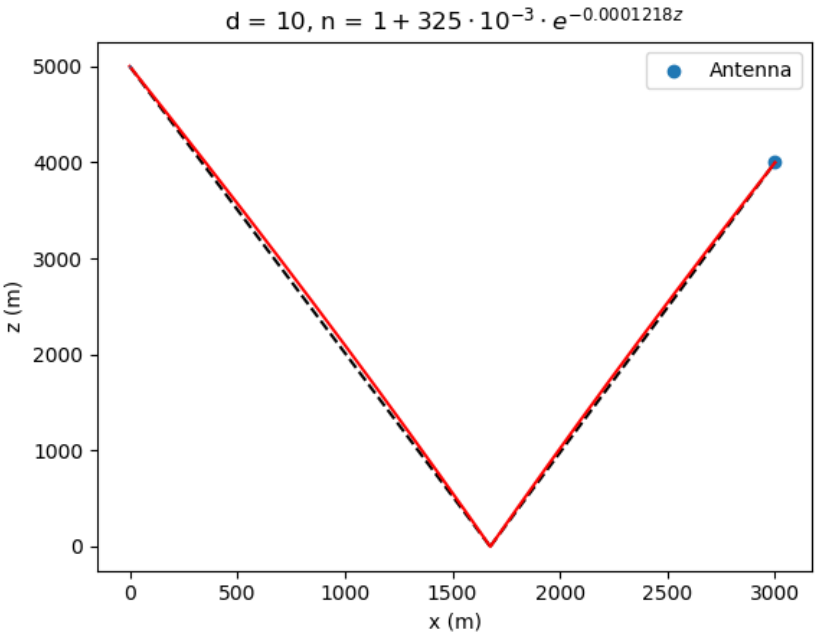

Figure 5.4: The path of a single ray through the atmosphere with layers of $d = 10m$. Here $\eta_0 = 325 \cdot 10^{-3}$ is used to exaggerate refraction. The black dotted line gives a straight trajectory.

5.3 Reflection and Mirages

Here we will discuss the importance of the reflection coefficients during the propagation and how the possibility for mirages is implemented in the code.

For reflection we can look at an arbitrary interface between air layers it will be shown that the reflection coefficients are negligible. Look at the reflection of the interface between air layers with refractive indices $n(h)$ and $n(h-d)$. Assuming the angle of incidence is θ and substituting these refractive indices in equations 4.8 and 4.9 results in the following reflection

coefficients

$$r_s = \frac{n(h)\cos\theta - n(h-d)\sqrt{1 - \frac{n(h)^2}{n(h-d)^2}\sin^2\theta}}{n(h)\cos\theta + n(h-d)\sqrt{1 - \frac{n(h)^2}{n(h-d)^2}\sin^2\theta}} \tag{5.7}$$

and

$$r_p = \frac{n(h)\sqrt{1 - \frac{n(h)^2}{n(h-d)^2}\sin^2\theta} - n(h-d)\cos\theta}{n(h)\sqrt{1 - \frac{n(h)^2}{n(h-d)^2}\sin^2\theta} + n(h-d)\cos\theta}. \tag{5.8}$$

The values of the r_s and r_p as a function of θ for $h = 1\text{m}$, $h = 1000\text{m}$ and $h = 10000\text{m}$ are plotted in figure 5.5.

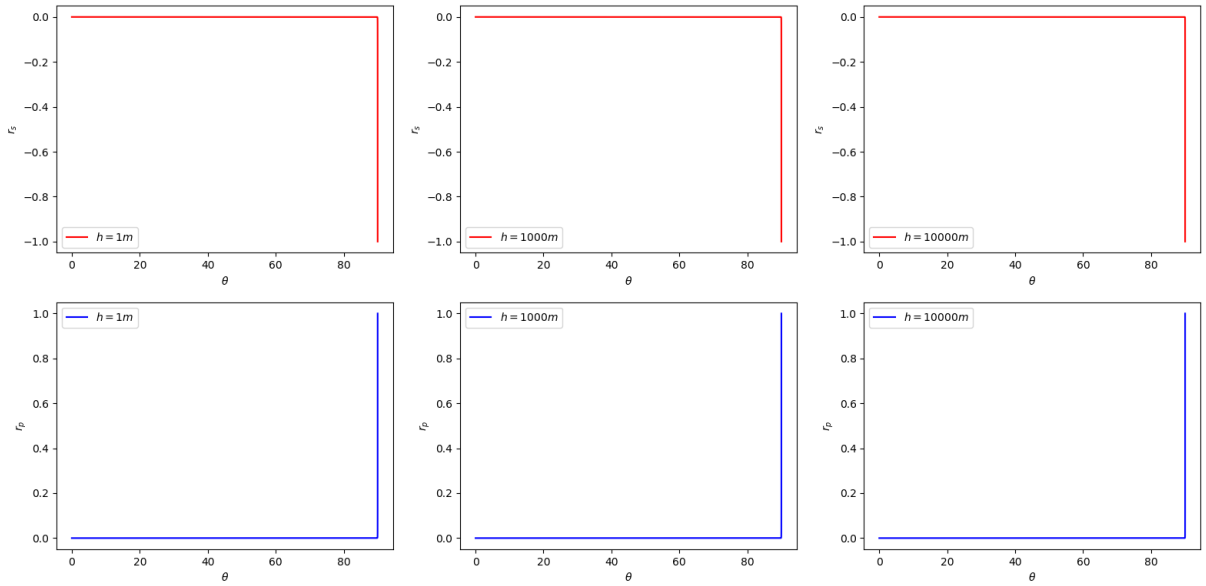

Figure 5.5: The reflection coefficients r_s (top) and r_p (bottom) as a function of angle of incidence, θ, for $d = 10\text{cm}$ and three different heights, $h = 1\text{m}$, $h = 1000\text{m}$ and $h = 10000\text{m}$.

Here we can see reflection of an arbitrary air layer plays no role in the case of the used model for the refractive index. It is therefore ignored.

Allowing for mirages in the simulation is a simple procedure. Since we assume the atmosphere to be a layered material, the model of equation 5.2 can be adjusted. We can define i values for which we choose a refractive index which differs from

$$n_i = 1 + \eta_0 e^{-\kappa\left(i+\frac{1}{2}\right)d}.$$

By taking new refractive indices for small i that are greater than those given by equation 5.2, a superior mirage can be simulated. The direction of an electromagnetic wave in a superior mirage is governed by Snell's law. Since the simulation calculates refraction at each interface between air layers, the possibility of a superior mirage is already accounted for.

Implementation of an inferior mirage needs some more work. Again the conditions for this type of mirage can be created by adjusting the refractive indices n_i. In the simulations the direction of the signal with these new refractive indices is still correctly calculated. There needs

to be one addition, which is the check whether or not the incident angle at each interface exceeds the critical angle for TIR. This can be reduced to one single check. Let $n_{incident}$ denote the refractive index in the air layer where a signal originates. The angle of incidence upon the first interface is θ. Using equation 4.14 and Snell's law, the condition for total internal reflection of the interface between the i-th and $i+1$-th layer is

$$\theta \geq \sin^{-1} \frac{n_i}{n_{incident}}. \tag{5.9}$$

If this criterion is fulfilled, we can determine the interface off which the signal will reflect. Taking into account the correct reflection coefficients the signal measured at the location of the antenna can be measured as layed out in section 5.6.

5.4 The Air Shower

With the path of a single ray calculated, the whole air shower can be simulated. Let the air shower be an emitter travelling at the speed of light along the shower axis at an angle θ with respect to the vertical z-axis. The components of the velocity vector are then

$$\mathbf{c} = \begin{pmatrix} c\sin\theta \\ 0 \\ -c\cos\theta \end{pmatrix} \tag{5.10}$$

We let the air shower emit a signal every Δt seconds. With this information, the location of emittance of every pulse is easily calculated. Let the first pulse be emitted at the location (x_0, z_0), then the i-th pulse originates from $(x_0 + c(i-1)\sin\theta, z_0 - c(i-1)\cos\theta)$. These coordinates can be used to iteratively calculate the path each individual pulse takes using the recurrence relations from section 5.2.

For the signal to be measured at a predetermined location of an antenna we need to calculate the angle between the signals and the shower axis, the off-axis angle Ψ. This requires constraints for Ψ. These constraints are easily found if we realise the last x coordinate found from equation 5.4 and the last z coordinate found from equation 5.6, should equal the x and z coordinates of the antenna, denoted by $x_{antenna}$ and $z_{antenna}$. If we let (x_N, z_N) denote the last coordinate pair found from the recurrence relation 5.4, 5.6 and 5.5, then x_N is given by

$$x_N = x_0 + c(i-1)\sin\theta + \sum_{\text{all path segments}} \frac{d\frac{n_{incident}}{n_t}\sin(\theta - \Psi)}{\sqrt{1 - \frac{n_{incident}^2}{n_t^2}\sin^2(\theta - \Psi)}}. \tag{5.11}$$

Here $n_{incident}$ corresponds to the refractive index of the first interface the signals crosses. n_t is the refractive index on the transmitted side of the considered term in the sum. If the coordinates of the antenna do not coincide with an interface the last term in the sum should be replaced by an expression that can be calculated in a similar fashion as equation 5.3. The same holds for the first term in the sum if z_0 does not coincide with an interface. With equation 5.11 and z_N, said criterion yields

$$\sqrt{(x_N - x_{antenna})^2 + (z_N - z_{antenna})^2} = 0. \tag{5.12}$$

Equation 5.12 can be solved numerically to find the off-axis angle for each individual ray. Having done this the situation for arbitrary z_0, x_0, Δt, $z_{antenna}$ and $x_{antenna}$ can be simulated, see figure 5.6.

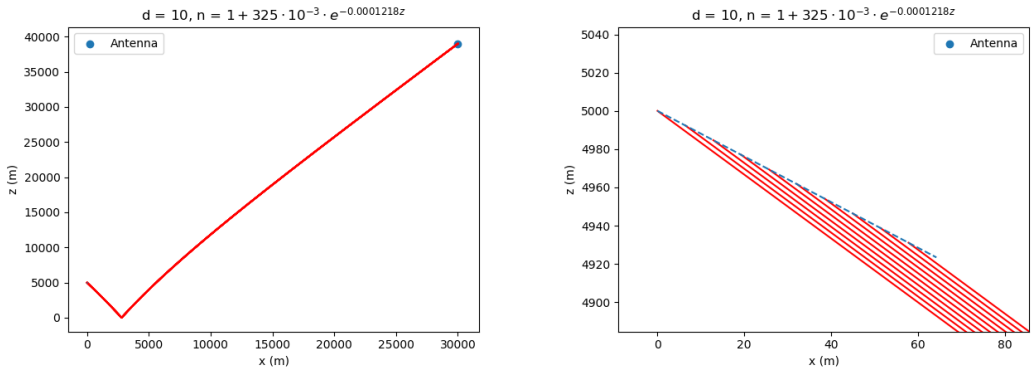

(a) (b)

Figure 5.6: In figure (a) the path of the signals from an air shower is plotted for $(x_0, z_0) = (0, 5000)$, $\Delta t = 3.34 \cdot 10^{-8}$s, $\theta = 40°$ and $(x_{antenna}, z_{antenna}) = (30000, 37000)$. The signal of the air shower consist of ten individual signals. In panel (b) a close up of the origin of the signal is shown, here all individual signals can be seen.

5.5 Implementing the Electric Field

Our simulated antenna will measure the amplitude of the electric field of a radio signal, as does ANITA. Thus, the electric field needs to be determined. From section 2 we know the electric field will be polarized in the $-\frac{\mathbf{v}\times\mathbf{B}}{|\mathbf{v}\times\mathbf{B}|}$ direction, i.e.

$$\mathbf{E} \propto -\frac{\mathbf{v}\times\mathbf{B}}{|\mathbf{v}\times\mathbf{B}|} \tag{5.13}$$

Since we assume the air shower to propagate at velocity c at an angle θ with the z-axis, the velocity vector is given by equation 5.14

$$\mathbf{v} = c\sin\theta\hat{\mathbf{x}} - c\cos\theta\hat{\mathbf{z}}. \tag{5.14}$$

For now the geomagnetic field is taken to be an arbitrary field, i.e. $\mathbf{B} = B_x\hat{\mathbf{x}} + B_y\hat{\mathbf{y}} + B_z\hat{\mathbf{z}}$. From this we can find the electric field at the point of emission,

$$\mathbf{E} \propto \frac{1}{\sqrt{c^2B_y^2 + (cB_z\sin\theta + cB_x\cos\theta)^2}} \begin{pmatrix} -cB_y\cos\theta \\ -cB_z\sin\theta - cB_x\cos\theta \\ -cB_y\sin\theta \end{pmatrix}. \tag{5.15}$$

When sending out the electric field from equation 5.15 at an off axis angle Ψ we get $\mathbf{k}\cdot\mathbf{E} \neq 0$, which is problematic since Maxwell's equations demand the dot product of the two to be zero. To solve this we rotate the electric field such that this condition is fulfilled. The angles Ψ are such that this only amounts to a very small rotation. The electric field for each individual pulse is then

$$\mathbf{E} \propto \frac{1}{\sqrt{c^2B_y^2 + (cB_z\sin\theta + cB_x\cos\theta)^2}} \begin{pmatrix} -cB_y\cos(\theta-\Psi) \\ -cB_z\sin(\theta-\Psi) - cB_x\cos(\theta-\Psi) \\ -cB_y\sin(\theta-\Psi) \end{pmatrix}. \tag{5.16}$$

The oscillatory behaviour of the electric field of equation 4.4 is ignored here, as it will be contained in the delta function that will be used in section 5.6. The electric field of equation 5.16 can now be decomposed in the two polarizations of figure 4.1, here we will dismiss the proportionality sign.

$$\begin{aligned}\mathbf{E}^{(p)} &= \frac{-cB_y\cos(\theta-\Psi)\hat{\mathbf{x}} - cB_y\sin(\theta-\Psi)\hat{\mathbf{z}}}{\sqrt{c^2B_y^2 + (cB_z\sin\theta + cB_x\cos\theta)^2}} \\ \mathbf{E}^{(s)} &= \frac{-\left(cB_z\sin(\theta-\Psi) + cB_x\cos(\theta-\Psi)\right)\hat{\mathbf{y}}}{\sqrt{c^2B_y^2 + (cB_z\sin\theta + cB_x\cos\theta)^2}}\end{aligned} \tag{5.17}$$

The goal now is to determine the electric field at the location of the antenna given equation 5.17. Substitution of the amplitudes $E^{(p)}$ and $E^{(s)}$ in equation 4.5 allows us to determine the transmitted field at the point of reflection. It needs to be noted that the positive and negative direction of $\mathbf{E}^{(p)}$ and $\mathbf{E}^{(s)}$ are arbitrary and depend on the choice of coordinate system. It is only the relative minus sign upon a phase shift of π that plays a role. It is therefore that we define the amplitudes $E^{(p)}$ and $E^{(s)}$ as

$$\begin{aligned}E^{(p)} &\equiv -\left|\mathbf{E}^{(p)}\right| \\ E^{(s)} &\equiv -\left|\mathbf{E}^{(s)}\right|\end{aligned} \tag{5.18}$$

From equation 4.5 and equations 4.10 and 4.11 we see that the electric field will be rotated at each interface as given by Snell's law. At each interface the s and p polarizations will pick up a factor t_s and t_p respectively. In the simulation these factors are ignored as both t_s and t_p are strictly positive and therefore don't change the phase of the signal. Both coefficients are also close to unity, and thus leave the amplitudes almost unaltered, see appendix B. Propagation through a layer also give rise to phase delay, which is given by [11]

$$\mathbf{E}(\mathbf{r}+\Delta\mathbf{r},\omega) = \mathbf{E}(\mathbf{r},\omega)e^{i\mathbf{k}\cdot\Delta\mathbf{r}}. \tag{5.19}$$

The phase delay is not explicitly calculated in the simulation, as the refractive index is assumed to be independent of frequency, it only gives rise to a time delay and no dispersion of the pulse, see appendix C for an explicit calculation.

For the reflection of the electric field we can use the appropriate Fresnel coefficients, r_s and r_p, to determine the amplitude and phase shift after reflection. Substituting this in equation 4.5 gives also the direction of the field. Using the reflected field as the new incident field, it can be propagated upwards through the atmosphere to the antenna. Having done this, the measured electric field at the antenna is

$$\mathbf{E}(\mathbf{r}_{antenna},t) \propto \begin{pmatrix} -r_pE^{(p)}\sqrt{1-\frac{n^2_{\text{incident}}}{n^2_{\text{antenna}}}\sin^2(\theta-\Psi)} \\ r_sE^{(s)} \\ r_pE^{(p)}\frac{n_{\text{incident}}}{n_{\text{antenna}}}\sin(\theta-\Psi) \end{pmatrix}\delta(t-t_i). \tag{5.20}$$

Here $E^{(p)}$ and $E^{(s)}$ are the components of the incident electric field as given by equation 5.18. The Fresnel coefficients are calculated for an incident signal in the first air layer reflecting off an ice sheet. With this electric field the signal measured by the antenna can be calculated.

5.6 The Measured Signal

The measured signal from each individual pulse is approximated by a delta function that is shifted in time, see equation 4.4.

$$A_i \propto \delta(t-t_i) \tag{5.21}$$

Here A_i denotes the measured amplitude of the signal and t_i the time delay of the signal. The proportionality is used, because equation 5.21 only includes the oscillatory behaviour of the

electric field and not the electric field vector itself. For each signal the time delay needs to be calculated. This is where the path of the signal comes in. The speed of light in a medium is given by $c' = \frac{c}{n}$ [11]. In this simulation the signal does not propagate at constant speed, each new layer induces a different propagation speed.

Since the goal is to simulate events as measured by ANITA, the signal needs to be passed through a band-pass filter that lets through frequencies in the range 200MHz $\leq \omega \leq$ 1200MHz. This can be realised by taking the Fourier transform of the signal followed by an inverse Fourier transform with the appropriate integration boundaries.

$$\mathcal{F}\{A_i\} = \frac{1}{\sqrt{2\pi}} \int_{-\infty}^{\infty} \delta\left(t - t_i\right) e^{i\omega t} dt \tag{5.22}$$

Equation 5.22 is easily evaluated to be

$$\mathcal{F}\{A_i\} = \frac{e^{i\omega t_i}}{2\pi}.$$

Taking the inverse Fourier transform with said boundaries gives the signal as measured by the antenna:

$$\int_{\omega_0}^{\omega_1} \frac{e^{i\omega t_i}}{\sqrt{2\pi}} e^{-i\omega t} \mathrm{d}\omega = \frac{\sin\left(\omega_1(t_i - t)\right) - \sin\left(\omega_0(t_i - t)\right)}{2\pi\left(t_i - t\right)} \tag{5.23}$$

Where $\omega_1 = 1200\text{MHz}$ and $\omega_0 = 200\text{MHz}$. Combining equations 5.20 and 5.23 signals of the two polarizations can be obtained.

$$\begin{aligned} \text{Vpol} &= r_p E^{(p)} \frac{\sin\left(\omega_1(t_i - t)\right) - \sin\left(\omega_0(t_i - t)\right)}{2\pi\left(t_i - t\right)} \\ \text{Hpol} &= r_s E^{(s)} \frac{\sin\left(\omega_1(t_i - t)\right) - \sin\left(\omega_0(t_i - t)\right)}{2\pi\left(t_i - t\right)} \end{aligned} \tag{5.24}$$

With this we can simulate the signal coming from an air shower. An example is shown in figure 5.7.

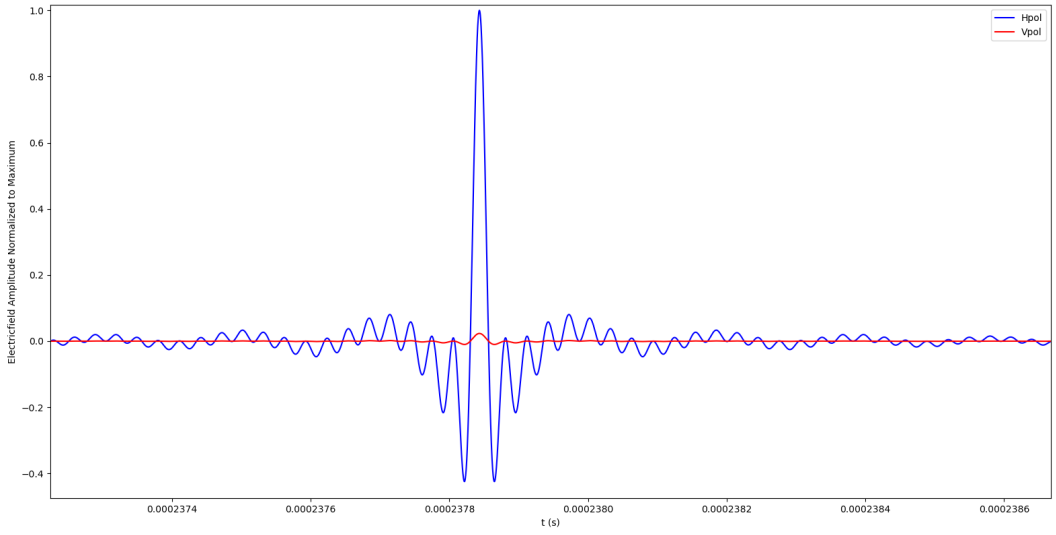

Figure 5.7: The signal as measured by the antenna in the simulation. Starting values are as follows: $x_0 = 0\text{m}$, $z_0 = 30\text{km}$, $x_{\text{antenna}} = 24.4\text{km}$, $z_{\text{antenna}} = 37\text{km}$, $d = 10\text{m}$, $\theta = 20°$, #Pulses= 100, $\Delta t = 3.34 \cdot 10^{-7}\text{s}$ and $\mathbf{B}$= 40mT$(0.01, 0.01, 1)$. The time origin, t=0, is the time the first signal from the air shower was emitted.

5.7 Total Internal Reflection

Now that we are able to simulate the signal from the air shower, the simulation is almost complete. As discussed in section 4.3, we should take into account the possibility of total internal reflection. In the case of total internal reflection we can take a closer look at r_p and r_s. From the first two equations of 4.13 we see that in the case of total internal reflection both r_s and r_p have absolute value 1. Beyond the critical angle, equation 4.14, the reflection (and transmission) coefficients become complex. This means they can be written as

$$r_s = e^{i\delta_s} \tag{5.25}$$

$$r_p = e^{i\delta_p} \tag{5.26}$$

The explicit form of these phases can be worked out from 4.8 and 4.9, using Snell's law we get [11]

$$r_s = \exp\left\{-2i \arctan\left(\frac{n_t}{n_i \cos_i}\sqrt{\frac{n_i^2}{n_t^2}\sin^2\theta_i - 1}\right)\right\} \tag{5.27}$$

$$r_p = -\exp\left\{-2i \arctan\left(\frac{n_i}{n_t \cos_i}\sqrt{\frac{n_i^2}{n_t^2}\sin^2\theta_i - 1}\right)\right\} \tag{5.28}$$

Now we need to look at how a phase shift due to reflection affects the measured signal. To do this we need to start with equation 4.4. Multiplying a reflection coefficient with the filtered delta function, equation 5.23, results in

$$\mathbf{E}(\mathbf{r},t) \propto e^{i\delta_{(p,s)}} \cdot \frac{\sin\left(\omega_1(t_i - t)\right) - \sin\left(\omega_0(t_i - t)\right)}{2\pi\left(t_i - t\right)} \begin{pmatrix} \mathrm{E}^{(p)} \\ \mathrm{E}^{(s)} \end{pmatrix} \tag{5.29}$$

If we multiply $e^{i\delta}$ with our signal of equation 4.3 and look at the real part, i.e. the actual electric field, this amounts to a phase shift of δ of the sine function. This results in equation 5.30.

$$\mathbf{E}(\mathbf{r},t) \propto \begin{pmatrix} \frac{\sin\left(\omega_1(t_i-t)+\delta_{(p)}\right)-\sin\left(\omega_0(t_i-t)+\delta_{(p)}\right)}{2\pi(t_i-t)}\mathrm{E}^{(p)} \\ \frac{\sin\left(\omega_1(t_i-t)+\delta_{(s)}\right)-\sin\left(\omega_0(t_i-t)+\delta_{(s)}\right)}{2\pi(t_i-t)}\mathrm{E}^{(s)} \end{pmatrix} \tag{5.30}$$

With this the simulation is complete, a link to the code is given in appendix E. In the next section we will look at the coherence of the measured signals.

5.8 Coherence in the Simulation

A good check for the simulation is to try and find a Cherenkov cone. For this we let our antenna be on the ground. There will be no reflection off the ice. The first signal of our air shower will be emitted at an altitude of 30km. From equation 4.17 we can estimate where we would expect a peak in the maximum measured amplitude. Using $n = 1.000325$ for the refractive index of air, we calculate the antenna location about $734m$ to the right of where the first signal originates to be the place where the signals are most coherent. As our refractive index is a function of height this is only an approximation. The results are given in figure 5.8.

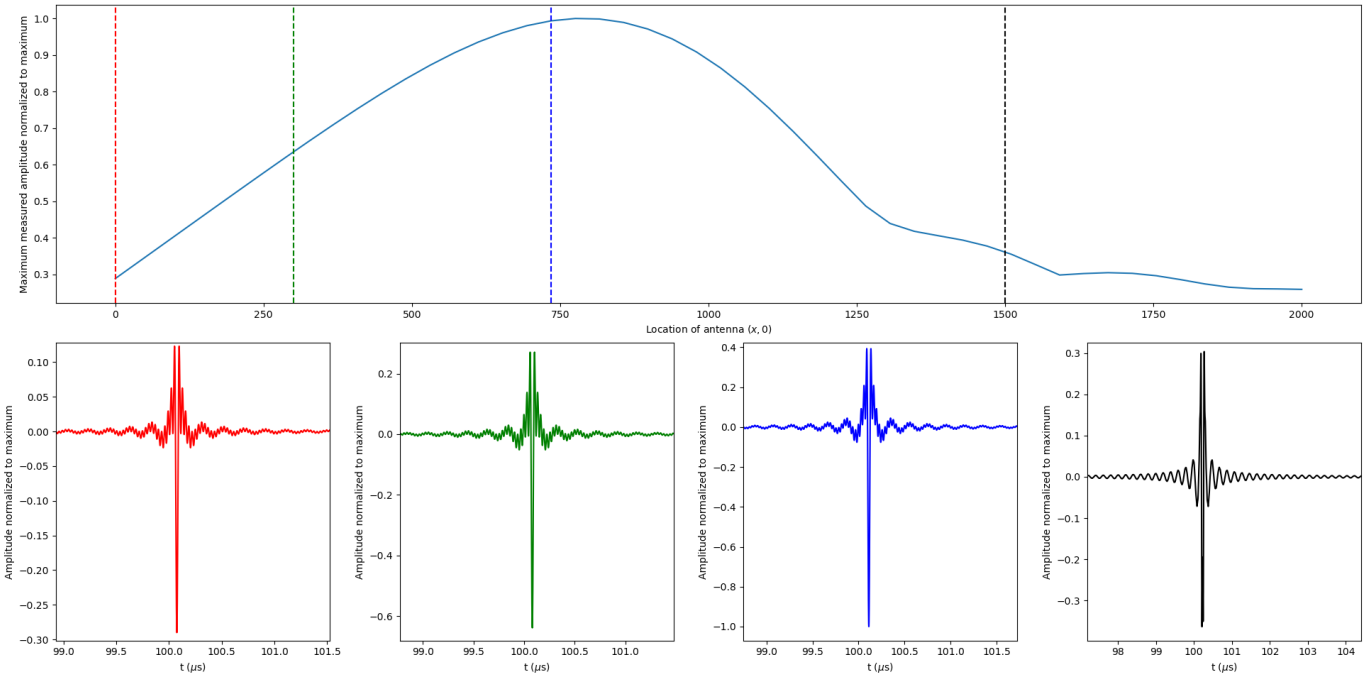

Figure 5.8: The maximum measured amplitude (top) and the measured signals at four distinct locations, normalized to the maximum of all the signals. Close to $x = 734m$ we see a peak that corresponds to the cherenkov angle.

This shows exactly what we would expect. The maximum measured amplitude peaks around the distance that corresponds to the Cherenkov angle. At $x = 0m$, $x = 300m$, $x = 734m$ and $x = 1500m$ the signals are shown. Here we see the strongest signal is found around the Cherenkov angle. Far away, at $x = 1500m$, we already start seeing two peaks. Here the signals are less coherent and we start seeing the individual signals instead of a coherent sum.

6 TIR as an Explanation For Anomalous ANITA Measurements

Now that the simulation is completed it is possible to start experimenting within the simulation to find possible solutions to the anomalous ANITA measurements. As mentioned earlier the goal is to find something in the propagation that explains the observations of the various ANITA flights. There are two obvious places to look. The first is the propagation through air. Since the Fresnel coefficients for transmission are always positive, there is no phase shift. Besides reducing the amplitude, these coefficients will not change the polarity of our signal. The other place to look is the reflection. As the reflection is what induces a phase shift of π it seems to be the place where the explanation could be found.

6.1 Total Internal Reflection and Phase Shift

For total internal reflection, i.e. when the incident angle exceeds the critical angle, the Fresnel coefficients become complex. These coefficients are then given by equations 5.27 and 5.28. For an ice to air interface the phase of the Fresnel coefficients for reflection are plotted in figure 6.1.

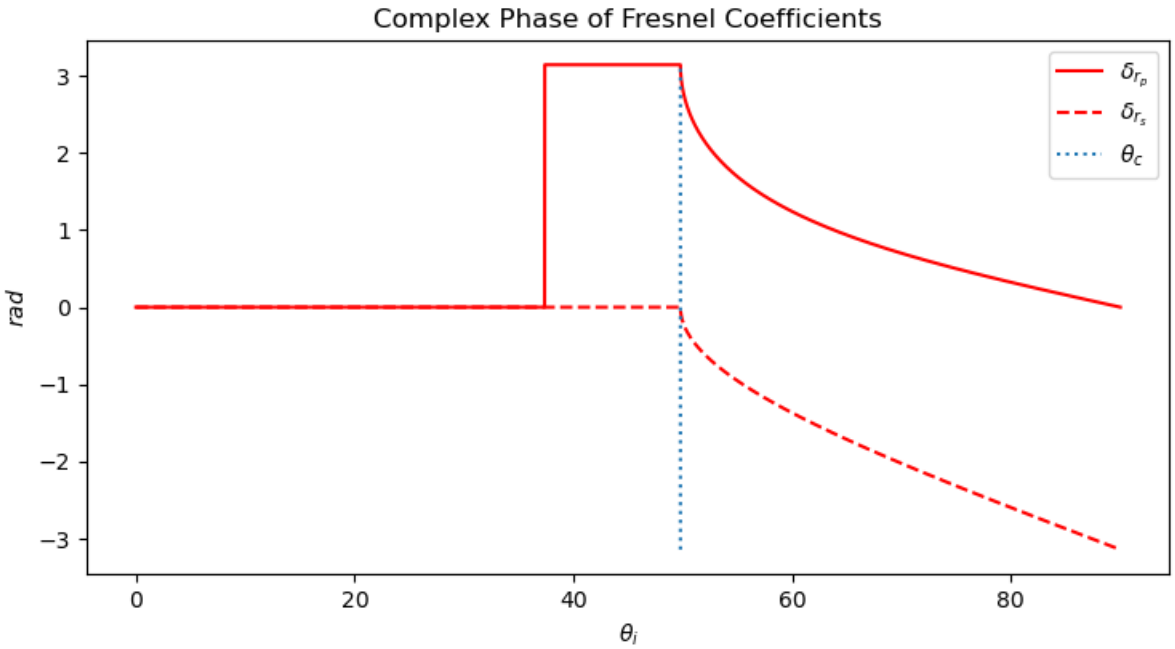

Figure 6.1: The phases of the reflection coefficients for a reflection off an air to ice interface.

The red and red dashed line give the phase of the r_p and r_s, respectively. The blue dotted line is the critical angle. In this figure we see two things that look interesting. First is what happens beyond the critical angle and what was also discussed in equations 5.27 and 5.28. Beyond the critical angle the phase shift is no longer restricted to π. This means that total internal reflection somewhere in the ice layer can be used to reflect a signal without necessarily inverting the polarity.

The second thing that we see in figure 6.1 is that for relatively small incident angles there is no phase shift at all.

Both of these cases give rise to the idea of having air trapped underneath the ice, such that we

can realise the ice to air interface.

6.2 Increasing Refractive Index of Ice

Another important aspect that will play a role in constructing situations where total internal reflection takes place has to do with the refractive index of ice.

The refractive index as a function of ice depth is not constant, rather it is an increasing function. The results of a measurement of the refractive index of ice in Greenland is shown in figure 6.2.

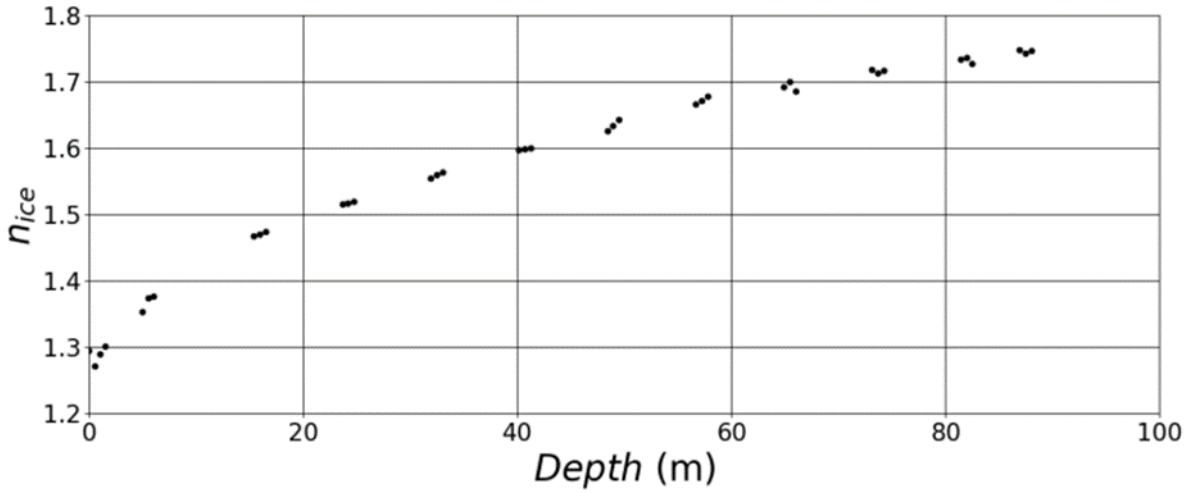

Figure 6.2: The refractive index as a function of depth [17]

With this, we can simulate the ice the same way we did the atmosphere, as a layered system of constant refractive indices.

The next section will use the concepts of this section to construct situations for which there is no inversion of the polarity of a signal upon 'reflection'.

7 Checking Different Geometries for TIR

In this section we will look at different geometries and check them for the possibility of an apparent reflection, but without a phase shift of π. The geometries are inspired by the things discussed in section 6. All scenarios in this section are some system of three layers with refractive indices n_1, n_2 and n_3. Even though all criteria that will be derived are valid for arbitrary refractive indices, limited to the obvious constraints such that TIR can occur, to make explicit calculations the following values will be used: $n_1 = n(20m)$ according to equation 5.1, $n_2 = 1.33$ and $n_3 = 1.000325$ unless n_3 corresponds to a material different from air or another value is explicitly given.

7.1 Horizontal Layers

The simplest geometry we can think of is a layered system of horizontal layers. Here we can just alter refractive indices to construct an air layer under the ice or an increasing refractive index of ice. Both of these scenarios can be regarded as a three layered system. These scenarios are shown in figure 7.1.

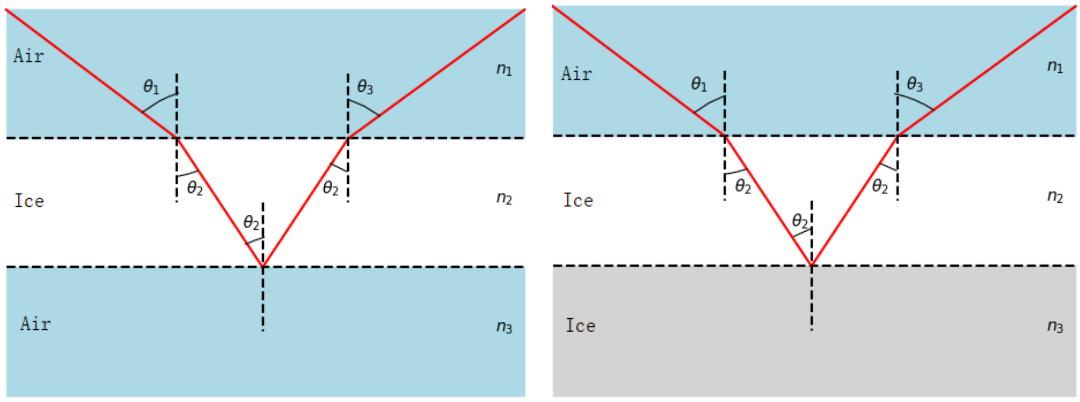

(a) (b)

Figure 7.1: In panel (a) there is an air pocket trapped underneath the ice and the signal reflects off the bottom ice-air interface. In panel (b) the same happens, but here the bottom layer is an ice layer with a refractive index n_3 greater than n_2.

Now we need to determine criteria for these situations to occur. First consider panel (a) in figure 7.1. First the signal is transmitted through the first interface, then TIR off the bottom interface followed by a transmission through the top interface. The angle of incidence upon the first interface is θ_1. Snell's law gives

$$n_1 \sin\theta_1 = n_2 \sin\theta_2.$$

From this the angle of incidence upon the bottom interface is given by

$$\theta_2 = \arcsin\left(\frac{n_1}{n_2}\sin\theta_1\right). \tag{7.1}$$

From the law of reflection follows that the incident angle upon the top interface is again θ_2. At this point we can construct two criteria

$$\begin{aligned} \theta_2 &= \arcsin\left(\frac{n_1}{n_2}\sin\theta_1\right) \geq \arcsin\left(\frac{n_3}{n_2}\right); \\ \theta_2 &= \arcsin\left(\frac{n_1}{n_2}\sin\theta_1\right) < \arcsin\left(\frac{n_1}{n_2}\right), \end{aligned} \tag{7.2}$$

where the first corresponds to TIR and the second to transmission.

From equation 7.2, we can conclude

$$\arcsin\left(\frac{n_1}{n_2}\right) > \arcsin\left(\frac{n_3}{n_2}\right)$$

must hold. Thus $n_1 > n_3$ is required. Using the model from equation 5.2 we get $n_3 > n_1$, from which we would conclude that this scenario cannot happen. Even in the case we would assume n_3 to be smaller than n_1, both of these would still be very near equal to each other resulting in, using equation 4.14, a near horizontal angle of incidence. This in turn would lead to a near horizontal angle θ_3, as $\theta_1 = \theta_3$, resulting in total internal reflection in the atmosphere. Therefore this scenario does not provide a solution to the problem.

An other option in this same system is the case of a normal reflection off this interface. From figure 6.1 we know this will result in no phase shift. As the simulation is already capable of simulating horizontal layered system, this scenario can be easily checked. Underneath the ice we simply add another air layer with $n = 1.000325$. We simulate this for the Brewster angle θ_B, then we know that there is no p polarization reflected. The result of this is shown in figure 7.2, compare this with figure 5.7.

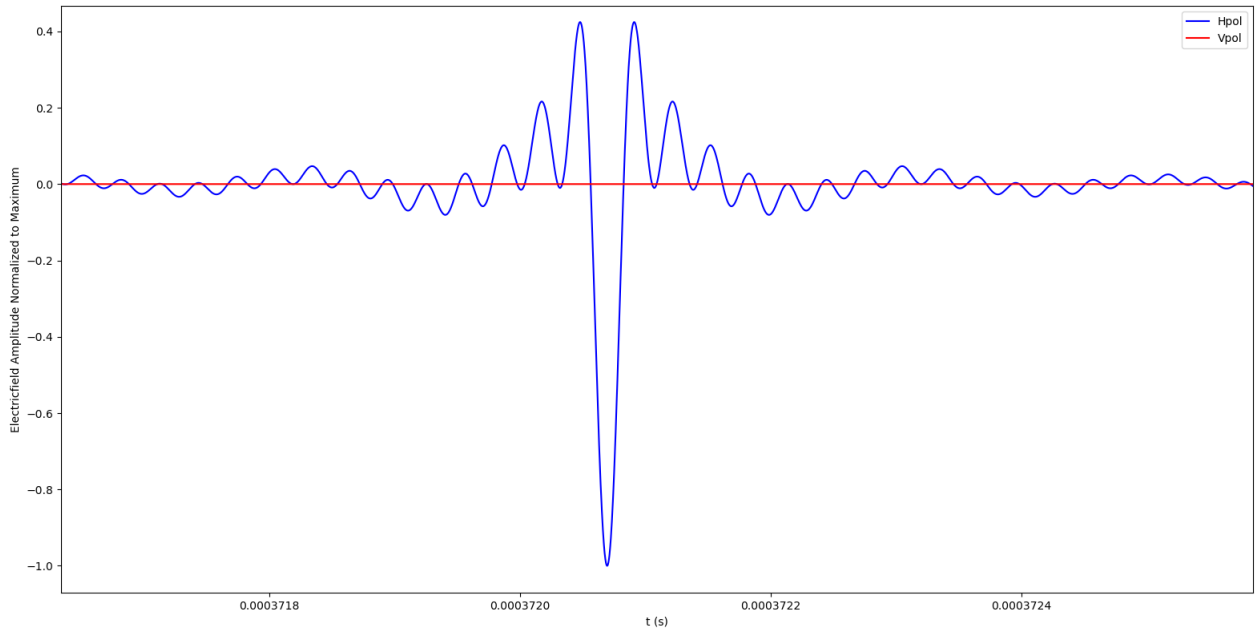

Figure 7.2: The signal after propagation as described in figure 7.1 (a). After comparison with figure 5.7 it is clear this signal is not inverted.

What has to be checked, though, is the amplitude of the signal after propagation through this system. As the transmission coefficients can exceed 1 in the case of propagation from a medium with greater refractive index to one with smaller refractive index, it is better to look at reflectance and transmittance. This gives us the fraction of power that is transmitted or reflected, see equations 4.13. The reflection coefficients for an air-ice and an ice-air interface are shown in figure 7.3.

From these we can determine the fraction of power that is lost with respect to the incoming power. Because phase shifts due to propagation just leads to a time delay of the delta function signal, we will ignore these and just multiply subsequent transmittance and/or reflection coefficients. Multiplying the two transmittance coefficients and reflectance coefficient for the

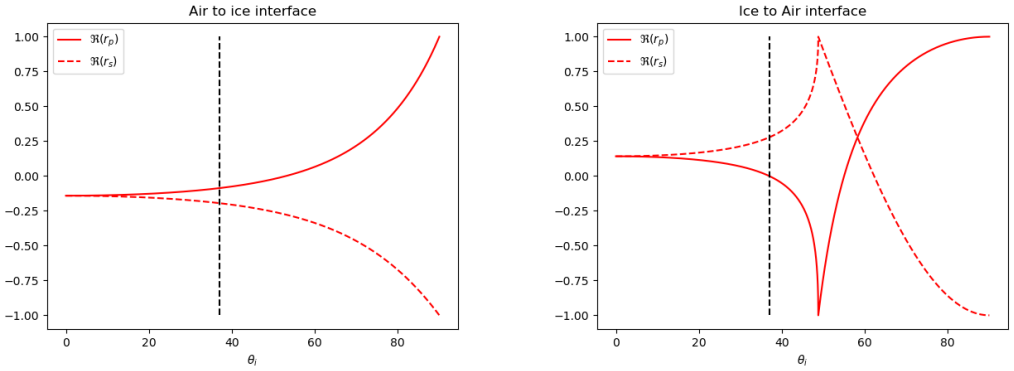

(a) Reflection coefficients air to ice interface (b) Reflection coefficients ice to air interface

Figure 7.3: The reflection coefficients for an air to ice interface (left) and an ice to air interface (right). The black dotted line indicates an angle of incidence equal to the Brewster angle for an ice to air interface.

path shown in figure 7.3a, calculated using equations 4.13 and figure 7.1, yields a power loss of 93.4% for the s polarization, which is too much for this scenario to be considered a solution to the problem.

The scenario of figure 7.1b does not give us the desired result. A normal reflection off the ice layer with greater refractive index gives a phase shift of π. Demanding total internal reflection from the top interface followed by an other reflection of the bottom also does not work. If the angles are such that we get said total internal reflection, then, by the the law of reflection, after the next reflection we get another total internal reflection. I.e. after total internal reflection in this case, we can never get a transmission through the top interface.

7.2 Inclined Ice Plane

Given the system with horizontal layers does not work, we can try an inclined ice layer. We let the ice layer be tilted by an angle α, for $\alpha \in [0, 90]$. Again we can have an air pocket under the ice, or an other ice layer with greater refractive index as the one on top, see figure 7.4.

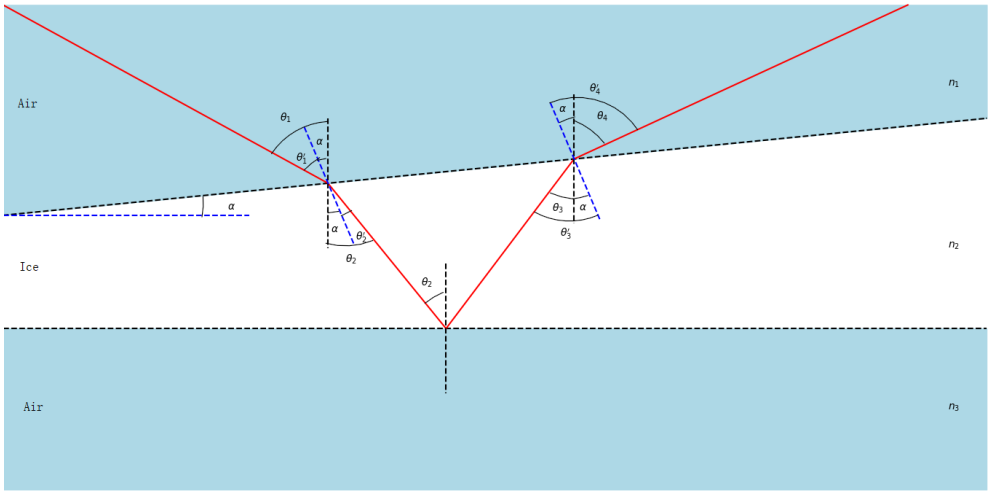

(a) Air pocket underneath the ice: $n_3 < n_2$

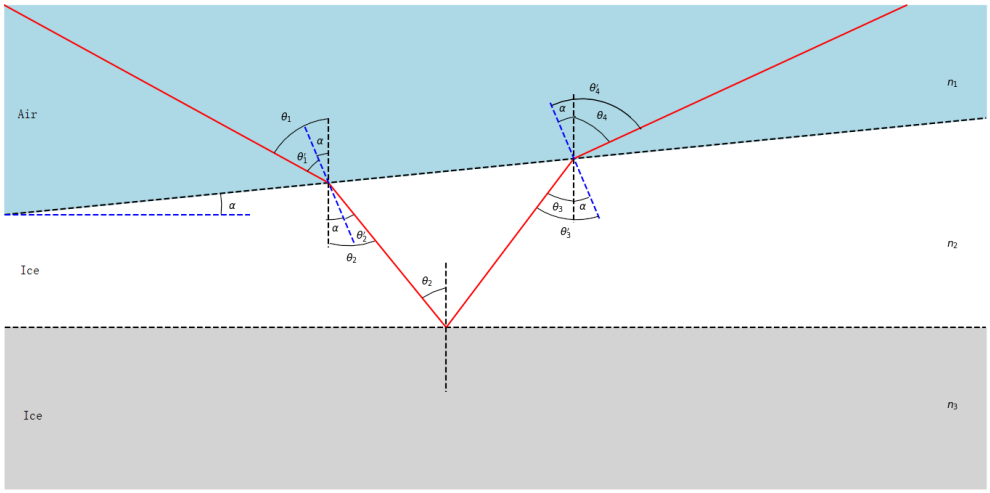

(b) Increasing refractive index of ice: $n_3 > n_2$

Figure 7.4: Layered system with an inclined ice surface at an angle α.

First consider the situation with the air pocket, figure 7.4a. By the law of reflection $\theta_3 = \theta_2$. Using Snell's law at the inclined surface we find

$$n_1 \sin \theta_1' = n_2 \sin \theta_2'.$$

From figure 7.4a follows: $\theta_{1,2}' = \theta_{1,2} - \alpha$. Substitution of this in Snell's law and solving for θ_2 yields

$$\theta_2 = \arcsin\left(\frac{n_1}{n_2} \sin\left(\theta_1 - \alpha\right)\right) + \alpha. \tag{7.3}$$

Again from figure 7.4a, $\theta_3' = \theta_2 + \alpha$. Now we can construct our criteria for this situation to occur. θ_2 should exceed the critical angle for total internal reflection at the bottom. θ_3' should be smaller than the critical angle, such that a transmission can occur. The two criteria are then as follows

$$\begin{aligned} \theta_2 &= \arcsin\left(\frac{n_1}{n_2} \sin\left(\theta_1 - \alpha\right)\right) + \alpha \geq \arcsin\frac{n_3}{n_2} \\ \theta_3' &= \arcsin\left(\frac{n_1}{n_2} \sin\left(\theta_1 - \alpha\right)\right) + 2\alpha < \arcsin\frac{n_1}{n_2} \end{aligned} \tag{7.4}$$

To have the biggest chance of fulfulling the second criteria of equation 7.4, we let the greater or equal sign in the first criterion be an equality. Substituting the right part of this equality in

the second criteria gives

$$\alpha < \arcsin\frac{n_1}{n_2} - \arcsin\frac{n_3}{n_2}. \tag{7.5}$$

Since $n_1 < n_2$ and $n_3 < n_2$, we get $\frac{n_1}{n_2}$, $\frac{n_3}{n_2} \in [0,1]$. Using our atmospheric model, equation 5.2, $n_1 < n_3$. Therefore $\frac{n_1}{n_2} < \frac{n_3}{n_2}$ and since $\arcsin x$ is strictly increasing for $x \in [0,1]$ the criteria from equation 7.4 demand $\alpha < 0$ and $-\alpha > \arcsin\frac{n_3}{n_2} - \arcsin\frac{n_1}{n_2}$. Note that this means that TIR is always followed by TIR, as the angle upon TIR from the top interface increases the angle with respect to the vertical by 2α.

We can allow for α to be negative by substituting $\alpha \to -\alpha$. Our criteria are then obtained from equation 7.4 by this substitution, see equation 7.6.

$$\begin{aligned}\theta_2 &= \arcsin\left(\frac{n_1}{n_2}\sin(\theta_1+\alpha)\right) - \alpha \geq \arcsin\frac{n_3}{n_2}\\ \theta_3' &= \arcsin\left(\frac{n_1}{n_2}\sin(\theta_1+\alpha)\right) - 2\alpha < \arcsin\frac{n_1}{n_2}\end{aligned} \tag{7.6}$$

Here the first criteria again corresponds to TIR off the bottom interface and the second to transmission through the top interface. The second criteria of equation 7.6 is always fulfilled. $\theta_1 \in [0, 90-\alpha]$, therefore $\forall_{\theta_1} 0 \leq \sin(\theta_1+\alpha) \leq 1$. From this follows

$$\arcsin\left(\frac{n_1}{n_2}\sin(\theta_1+\alpha)\right) - 2\alpha \leq \arcsin\left(\frac{n_1}{n_2}\right) - 2\alpha.$$

Together with our second criteria from equation 7.6 we get $\alpha > 0$. Note that for $\alpha = 0°$ we just get back to the situation of the previous section.

Now the first of these criteria must hold. The maximum of θ_2 is $\arcsin\frac{n_1}{n_2} - \alpha$. Then the first criteria becomes

$$\arcsin\frac{n_1}{n_2} - \alpha \geq \arcsin\frac{n_3}{n_2},$$

which is maximal for $\alpha = 0$. Then this criteria becomes $n_1 > n_3$. So for $n_1 > n_3$ this situation can occur. This can be realised if we consider equation 4.15. For the air pocket under the ice is cooled by the ice on top and there is an absence of sunlight. From this the temperature of the air under the ice is lower than immediately above the ice, giving rise to a lower refractive index. All criteria are then

$$\begin{cases} n_1 > n_3 \\ \arcsin\frac{n_1}{n_2} - \arcsin\frac{n_3}{n_2} \geq \alpha > 0 \\ \arcsin\left(\frac{n_2}{n_1}\sin\left(\arcsin\left(\frac{n_1}{n_2}\right)+2\alpha\right)\right) - \alpha > \theta_1 \geq \arcsin\left(\frac{n_2}{n_1}\sin\left(\arcsin\left(\frac{n_3}{n_2}\right)+\alpha\right)\right) - \alpha. \end{cases} \tag{7.7}$$

As this gives a very narrow region for θ_1, it is unlikely to explain all the anomalous ANITA measurements.

Now we can consider the case where $n_3 > n_2$, i.e. where the refractive index of ice increases with depth, figure 7.4b. Note that a single reflection just gives a phase shift of π. Therefore we need a reflection followed by TIR, followed by another reflection and then a transmission. For the TIR and transmission we can again find criteria. First θ_3' should exceed the critical angle, to get TIR. The law of reflection gives the angle of reflection: $\theta_3 + 2\alpha$ with respect to the vertical. Then after a reflection the angle of incidence upon the top interface will be $\theta_3 + 3\alpha$. As this is greater than $\theta_3 + 2\alpha \geq \arcsin\frac{n_1}{n_2}$ we again have TIR. Thus this does not work. If

we let $\alpha \in [-90, 0]$, i.e. $\alpha \to -\alpha$, the angle after TIR becomes smaller. The criteria for this situation are then (note that $\theta_2 = \theta_3$)

$$\begin{aligned} \theta_2 - \alpha &\geq \arcsin \frac{n_1}{n_2} \\ \theta_2 - 3\alpha &< \arcsin \frac{n_1}{n_2} \end{aligned} \tag{7.8}$$

where θ_2 is given by equation 7.3 with $-\alpha$ substituted for α. The maximum of θ_2 is $\arcsin \frac{n_1}{n_2} - \alpha$. Substituting this maximum in the second criteria of equation 7.8 we get

$$\arcsin \frac{n_1}{n_2} - 2\alpha < \arcsin \frac{n_1}{n_2}.$$

This implies that for $\alpha > 0$ the second criteria is always fulfilled. The first, however, is never satisfied, for

$$\begin{aligned} \arcsin\left(\frac{n_1}{n_2}\sin(\theta_1 + \alpha)\right) - 2\alpha &< \arcsin\left(\frac{n_1}{n_2}\sin(\theta_1 + \alpha)\right) \\ &\leq \arcsin \frac{n_1}{n_2}. \end{aligned}$$

Hence, this situation is also not possible.

7.3 Ice Sheet With Two Inclinations

Another situation we can check is given in figure 7.5.

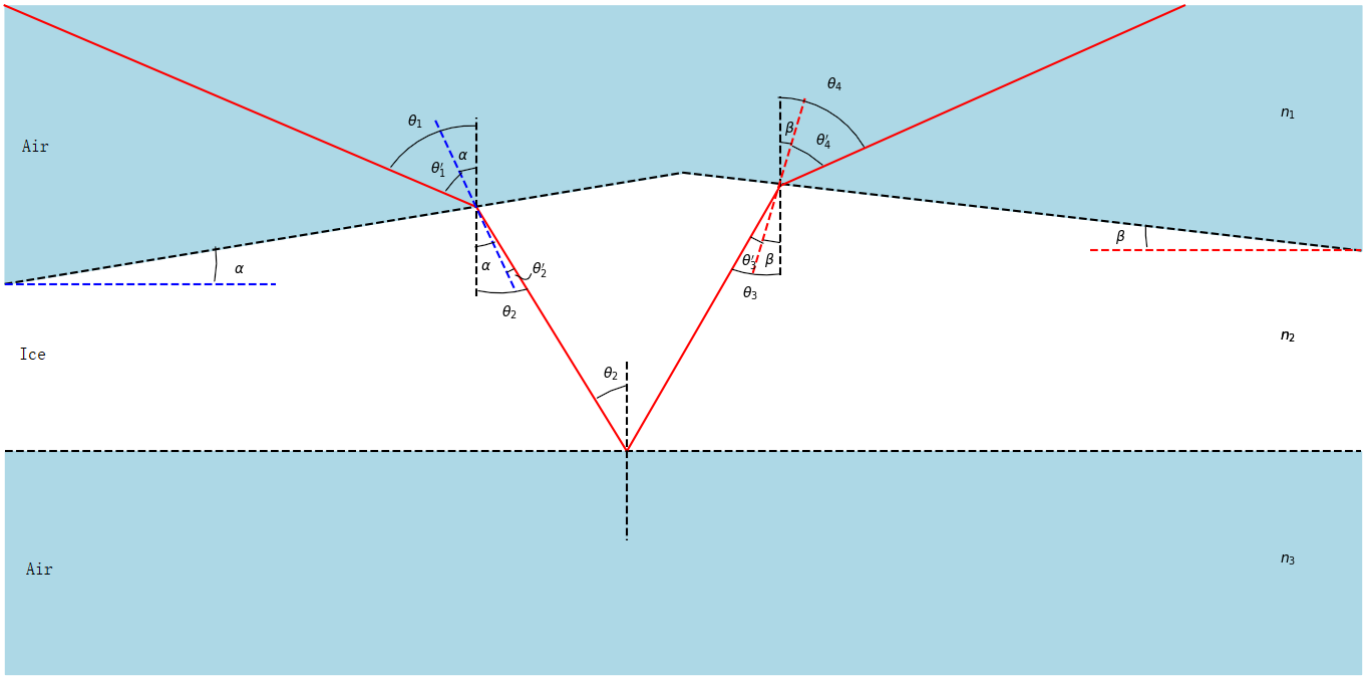

Figure 7.5: Layered system, with an air pocket under the ice and an ice sheet with two inclinations.

By allowing the ice to have two inclinations, we can use the first, α, to get a greater angle for total internal reflection and the second, β, such that the signal is transmitted. Where $\alpha, \beta \in [0, 90]$. Now the task at hand is again determining the criteria for this situation to occur. The angles in figure 7.5 are easily determined. Firstly

$$\theta_3 = \theta_2$$

by the law of reflection. Snell's law at the first interface gives

$$n_1 \sin\theta_1' = n_2 \sin\theta_2'.$$

Where $\theta_1' = \theta_1 - \alpha$ and $\theta_2' = \theta_2 - \alpha$. Hence

$$\theta_2 = \arcsin\left(\frac{n_1}{n_2}\sin\left(\theta_1 - \alpha\right)\right) + \alpha, \tag{7.9}$$

and

$$\theta_3' = \arcsin\left(\frac{n_1}{n_2}\sin\left(\theta_1 - \alpha\right)\right) + \alpha - \beta. \tag{7.10}$$

θ_2 should be greater than or equal to the critical angle at the bottom interface to get TIR and θ_3' should be smaller than the critical angle at the top interface to be transmitted. This results in two criteria

$$\begin{aligned} \arcsin\left(\frac{n_1}{n_2}\sin\left(\theta_1 - \alpha\right)\right) + \alpha &\geq \arcsin\frac{n_3}{n_2} \\ \arcsin\left(\frac{n_1}{n_2}\sin\left(\theta_1 - \alpha\right)\right) + \alpha - \beta &< \arcsin\frac{n_1}{n_2} \end{aligned} \tag{7.11}$$

The first of these criteria gives a lower bound for the angle of incidence θ_1. Solving for θ_1 in this criteria results in

$$\theta_1 \geq \arcsin\left(\frac{n_2}{n_1}\sin\left(\arcsin\left(\frac{n_3}{n_2}\right) - \alpha\right)\right) + \alpha \tag{7.12}$$

For this angle to exist the absolute value of the argument of the arcsine should be less than or equal to 1.

$$\frac{n_2}{n_1}\sin\left(\arcsin\left(\frac{n_3}{n_2}\right) - \alpha\right) \leq 1 \tag{7.13}$$

This puts a restriction on α,

$$\alpha \geq \arcsin\frac{n_3}{n_2} - \arcsin\frac{n_1}{n_2}.$$

The same can be done for the second criteria of equation 7.11, which puts an upper bound on the angle of incidence θ_1. Solving for θ_1 here yields

$$\theta_1 < \arcsin\left(\frac{n_2}{n_1}\sin\left(\arcsin\left(\frac{n_1}{n_2}\right) - \alpha + \beta\right)\right) + \alpha. \tag{7.14}$$

Again demanding the argument of the arcsine to be less than 1 gives

$$\frac{n_2}{n_1}\sin\left(\arcsin\left(\frac{n_1}{n_2}\right) - \alpha + \beta\right) \leq 1,$$

which results in the criteria $\alpha > \beta$. It needs to be noted that this criteria only is necessary if the second criteria of equation 7.11 does not hold everywhere. For $\alpha \leq \beta$, this criteria holds for all angles θ_1. The last important thing we should consider are the lower and upper bounds on θ_1 that follow from equations 7.14 and 7.12. The upper bound must be greater than the lower bound for there to be an angle θ_1 which satisfies the criteria. From this follows that

$$\beta > \arcsin\frac{n_1}{n_2} - \arcsin\frac{n_3}{n_2}.$$

Note that this criteria is only necessary if $n_3 < n_1$, because if $n_1 < n_3$ this lower bound on β is negative and we already require $\beta \geq 0$

All these criteria together give

$$\begin{cases} \alpha \geq 0 & n_3 \leq n_1 \\ \alpha > \arcsin\frac{n_3}{n_2} - \arcsin\frac{n_1}{n_2} & n_3 > n_1 \\ \beta \geq 0 & n_3 \geq n_1 \\ \beta > \arcsin\frac{n_1}{n_2} - \arcsin\frac{n_3}{n_2} & n_3 < n_1 \\ \arcsin\left(\frac{n_2}{n_1}\sin\left(\arcsin\left(\frac{n_1}{n_2}\right) - \alpha + \beta\right)\right) + \alpha > \theta_1 \geq \arcsin\left(\frac{n_2}{n_1}\sin\left(\arcsin\left(\frac{n_3}{n_2}\right) - \alpha\right)\right) + \alpha & \alpha > \beta \\ 90 + \alpha \geq \theta_1 \geq \arcsin\left(\frac{n_2}{n_1}\sin\left(\arcsin\left(\frac{n_3}{n_2}\right) - \alpha\right)\right) + \alpha & \alpha \leq \beta \end{cases} \tag{7.15}$$

From these criteria we see the dependence on α and β of the bounds on θ_1. These dependencies can be graphically represented, see figure 7.6. Note that the maximum angle never exceeds 90°. It is possible for incident angles greater than 90° to fulfill all the criteria, but these angles would correspond to upward travelling signals, which we do not consider here.[ii] From this we can conclude that this scenario is restricted to relatively large zenith angles of the signal.

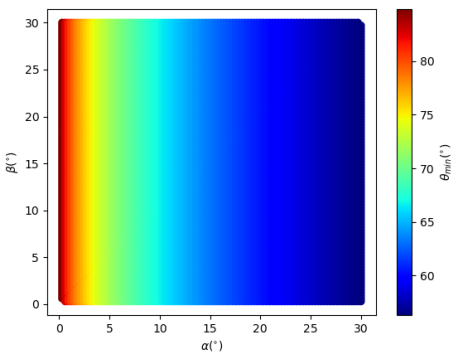

(a) $\theta_1 \geq \theta_{\min}$

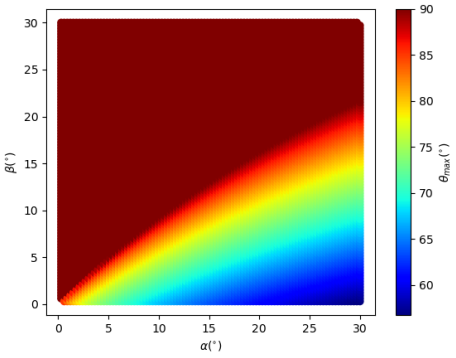

(b) $\theta_1 < \theta_{max}$

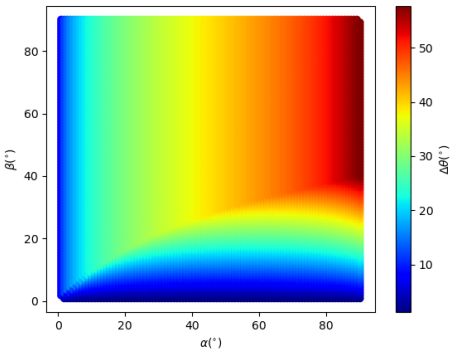

(c) $\Delta\theta = \theta_{max} - \theta_{min}$

Figure 7.6: Minimum and maximum values and range for angle of incidence θ_1 for all the criteria to be satisfied as a function of α and β.

[ii]The same holds for the rest of the scenarios considered in this thesis. We only look for angles $\theta_1 \leq 90°$ even if the criteria allow for greater angles.

7.3.1 Constraints on the Geometry

We know this situation works for one single ray, but we must make sure it can work for all the signals from the air shower. This can put constraints on the geometry of the ice. All signals need to be incident on the first inclined plane with inclination α. After TIR all the signals must leave the ice via the second inclined plane with angle β. As the distance between the first and last signal from the air shower is the biggest, these two are the only ones needed to find the constraints. We need to find lower bounds for a, b and h, see figure 7.7.

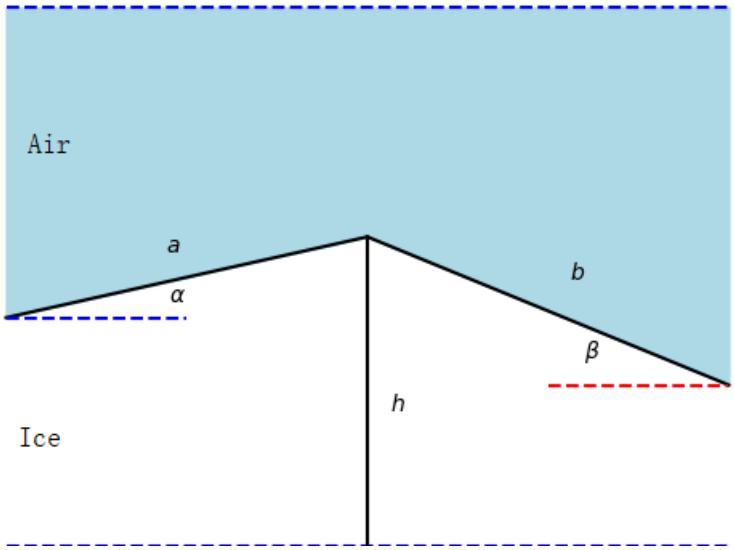

Figure 7.7: The defining lenghts of the geometry.

We first start with finding a lower bound for a. For this we need the distance between the first and last signal upon incidence on the ice sheet. When the two signals are transmitted we know the exact locations where these originate, see section 5.4. These are points A and B in figure 7.8. This distance is equal to the length of the air shower. For zenith angles of the air shower unequal to 0°, this distance is not the horizontal distance. It is this latter distance that is useful for finding a lower bound for a. To obtain this we let the last signal propagate to where it first intersects an interface between air layers, point D in figure 7.8. Then, we let the first signal propagate to this same interface, point C, and denote the horizontal distance there by ℓ_0. After propagation through the atmosphere the last signal will intersect the ice sheet, point E. The horizontal distance at this point, between E and F, will be denoted by ℓ. As the refractive index increases with each layer, the signal is refracted towards the normal. It will never 'cross' the normal. Because of this we can project point E straight down on the ice sheet, while being sure this gives a correct lower bound on a, albeit a somewhat greater lower bound than necessary. The lower bound on a is now easily calculated

$$a \geq \ell \cos \alpha \tag{7.16}$$

Remember that the simulation calculates each point where a signal intersects an interface, distances such as ℓ_0 and ℓ are therefore easily obtained from the simulation.

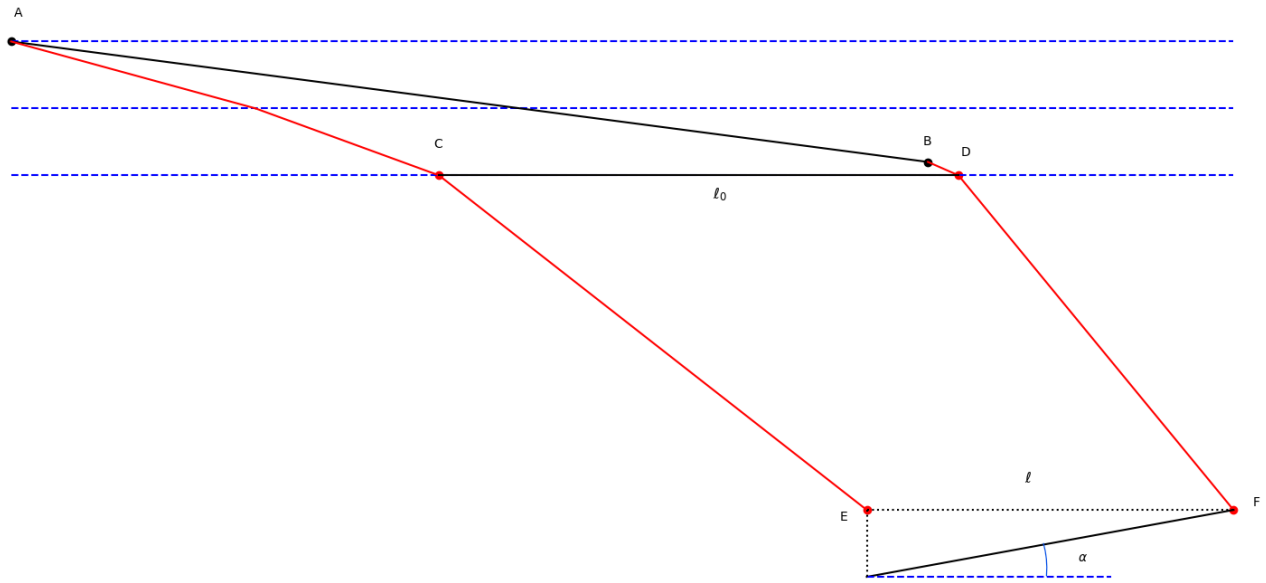

Figure 7.8: Horizontal distance between two signals during propagation to the ice.

The next step is the lower bound on h. The height h should be such that the first signal entering the ice should exit the ice a minimum distance of $a\cos\alpha$ further, see figure 7.9. In figure 7.9 this corresponds with the condition

$$x_1 + x_2 > a\cos\alpha. \tag{7.17}$$

x_1 and x_2 are easily obtained from the figure

$$\begin{aligned} \tan\theta_2 &= \frac{x_1}{h - a\sin\alpha} \\ \tan\theta_2 &= \frac{x_2}{h}. \end{aligned} \tag{7.18}$$

Solving equations 7.18 for x_1 and x_2, substituting $x_1 + x_2$ in equation 7.17 and solving for h, results in

$$h > \frac{a\cos\alpha}{2\tan\theta_2} + \frac{a\sin\alpha}{2}. \tag{7.19}$$

We only need to find an expression for θ_2. This is again given by equation 7.9.

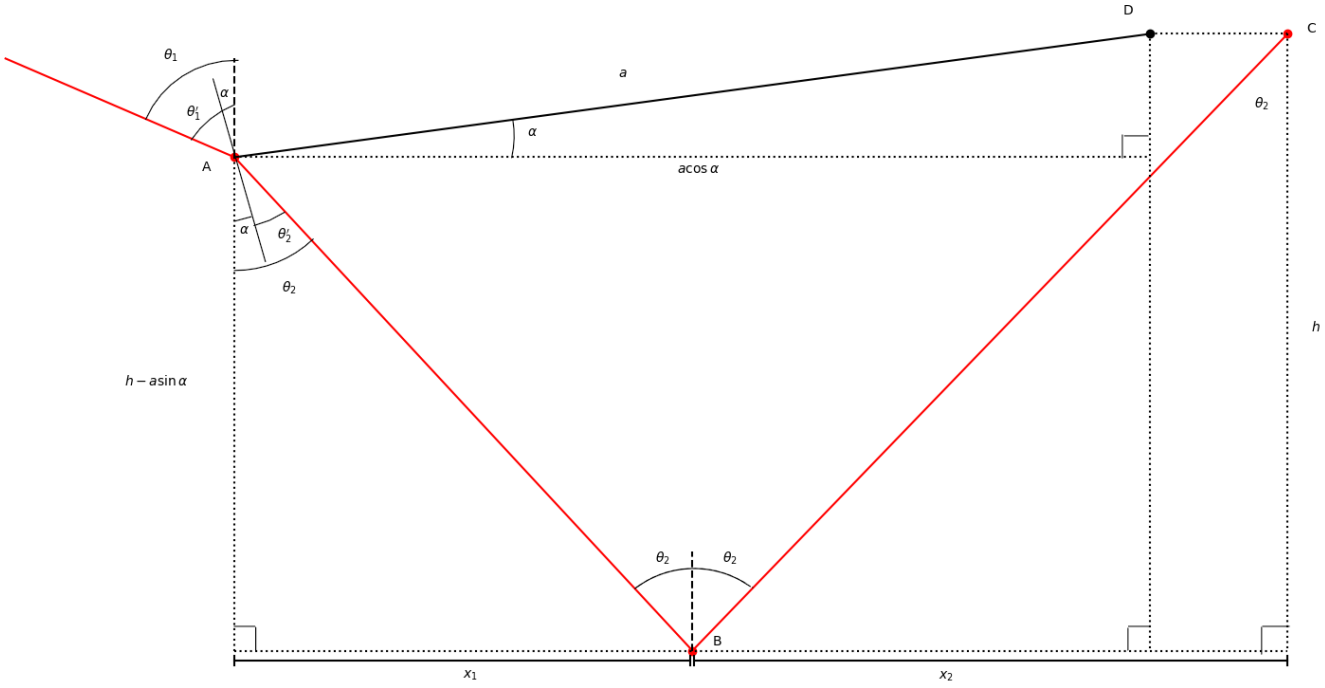

Figure 7.9: The first signal travelling through the ice layer.

The last constraint that needs to be found is the lower bound on b. For this we need the last signal. This one will come the farthest to the right of the first, and will thus determine the minimum length of b see figure 7.10

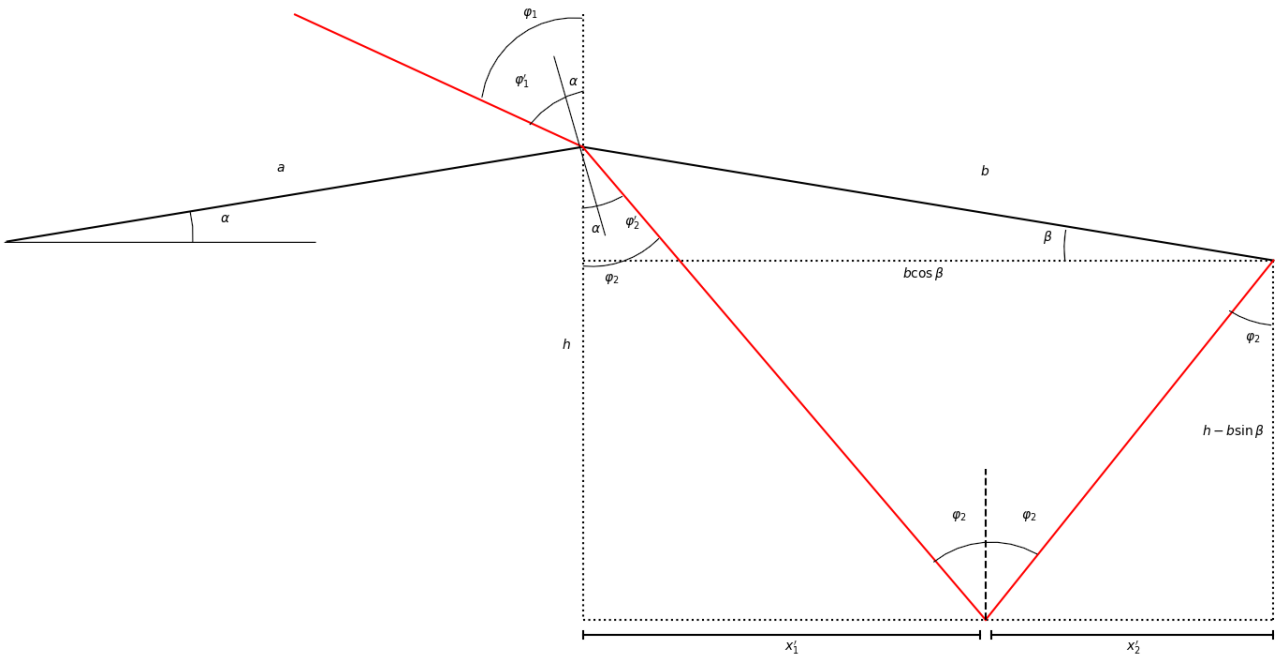

Figure 7.10: The last signal travelling through the ice layer.

Here we find the criteria for b, in a similar way we did for a. We demand

$$x_1' + x_2' < b\cos\beta. \tag{7.20}$$

Finding x_1' and x_2' is again a matter of simple geometry, they are given by the following expres-

sions

$$\begin{aligned} x_1' &= h \tan \varphi_2 \\ x_2' &= (h - b \sin \beta) \tan \varphi_2. \end{aligned} \tag{7.21}$$

Substitution of these expression in our criteria and solving for b yields a lower bound for b

$$b > \frac{2h \tan \varphi_2}{\cos \beta + \sin \beta \tan \varphi_2}. \tag{7.22}$$

The signal is incident on the first inclination, α. Therefore φ_2 is given by the same equation as θ_2 before, i.e.

$$\varphi_2 = \arcsin\left(\frac{n_1}{n_2} \sin\left(\varphi_1 - \alpha\right)\right) + \alpha. \tag{7.23}$$

To get an idea of how big these lower bounds are we can calculate them for a specific example. Let $\alpha = \beta = 4°$. We will express the criteria in terms of a. For the minimum angle of incidence θ_1 for this situation to occur, and assuming the signals to be parallel we find

$$h > 0.47a$$

and

$$b > a.$$

For the simulation we will do in the next section $a \approx 6.4m$.

7.3.2 Running the Simulation

Now we can run the simulation, and see if we get the desired result. We simulate for an angle of $\theta = 80°$ of the shower axis.

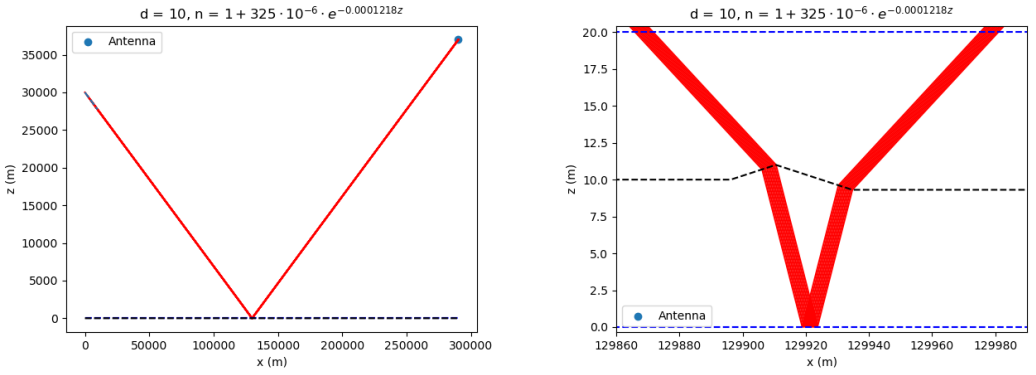

(a) (b)

Figure 7.11: The paths of the signals for ice with a hill with two inclinations.

The angles α and β are taken to be 4°. In figure 7.11b, which is figure 7.11a zoomed in, we can see clearly the signals propagate through the inclined ice sheet. The important thing to look at is the signal. For this we first need to think where we would expect coherence. For $\alpha = \beta$ we would expect it to be at approximately the same place as with the horizontal ice plane. The measured signal is shown in figure 7.12, together with a signal with the same starting conditions, but reflected from a horizontal ice sheet. This is exactly what we want to see. The measured signal is coherent, we see only one signal which is a superposition of all individual signals, and it is non inverted. From this we can conclude that this scenario produces a non inverted signal that would appear to be reflected off the ice. For this specific scenario

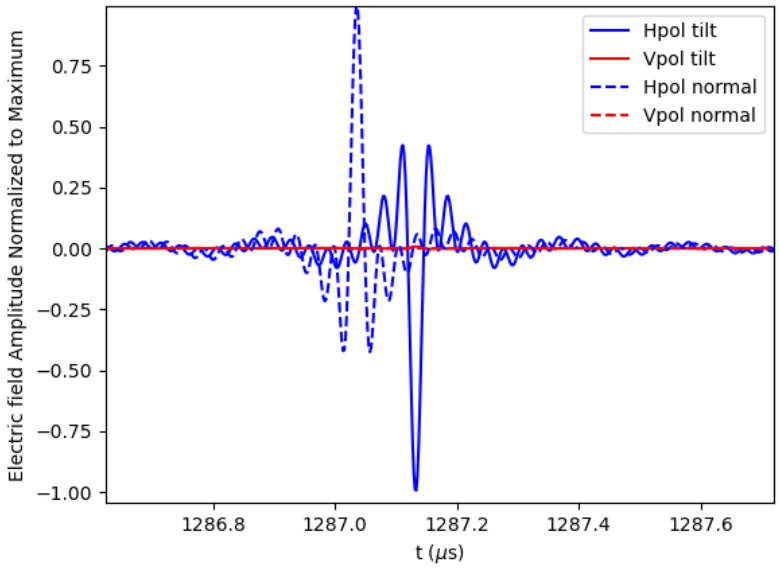

Figure 7.12: The measured signal at the antenna for signals travelling through ice with a hill with two inclinations (solid lines). Also the signal for an air shower with the same initial conditions but a signal reflected off a horizontal ice sheet (dashed lines).

we can determine the power loss. From the values for the angles extracted from the simulation we find a power loss of about 55% for the s polarization and 24% for the p polarization. Note that the amplitude is close to that off the 'normal' signal, which loses about 54.5% of the s polarization.

From figure 7.6, we know this situation is restricted to relatively big zenith angles. So this will not provide us with an explanation for the anomalous events seen during ANITA-I and ANITA-III. This could, however, provide an explanation to the events of ANITA-IV. These events are characterized by arrival angles of about 84° with respect to the vertical [9]. We can look for angles α and β and try to find the situation for which this would occur. We are after an angle $\theta_4 \approx 84°$, see figure 7.5. Using Snell's law we can calculate θ_1 in terms of α and β. We find

$$\theta_4 = 84° = \sin^{-1}\left(\frac{n_2}{n_1}\sin\left(\theta_2 - \beta\right)\right) + \beta, \tag{7.24}$$

where θ_2 is given in equation 7.9. Solving for θ_1 here, remember that θ_2 is a function of θ_1, and calculating the angle such that $\theta_4 = 84°$ results in figure 7.13. The percentage of power of the s polarization that is lost after propagation through the three layered is also shown.

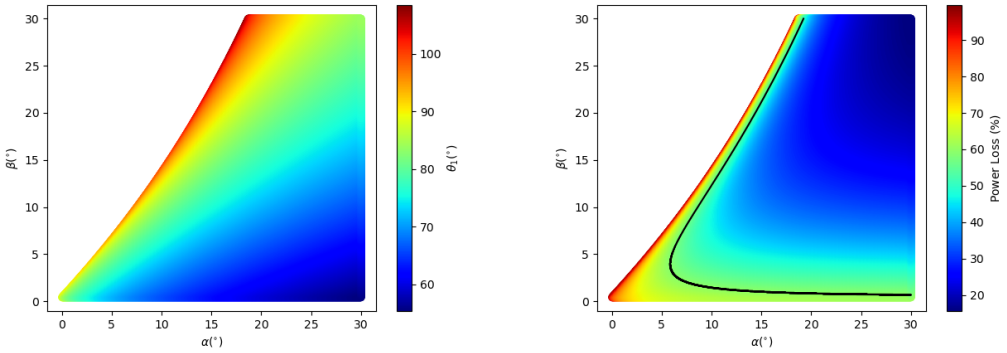

(a) θ_1 such that $\theta_4 = 84°$.

(b) Power loss in percent, for signal at incident angle θ_1.

Figure 7.13: Angle θ_1 and power loss of the s polarization as a function of α and β for arrival angle $\theta_4 = 84°$.

The black curve represents the 60% power loss contour. Here we see that for relatively small angles α and β we can already reduce the power loss to 60% (both angles slightly bigger than 5°). Therefore if ice structures like these are present in Antarctica, this could explain the anomalous ANITA-IV measurements.

7.3.3 A Normal Reflection

Now we will focus on the anomalous ANITA-I and ANITA-III measurements. With TIR we are restricted to relatively big angles for θ_1. The problem of big angles can possibly be resolved if we again consider figure 6.1. For all angles smaller than the critical angle, the s polarization does not get a phase shift upon reflection from a material with lower refractive index. As this is the most important polarization we can ignore the phase shift of π of the p polarization. With this in mind we can have a normal reflection off our ice pocket instead of TIR as in the previous subsection. The reason to look for angles close to the critical angle is because of figure 7.3. The reflection coefficient increases for greater angles. Now we can use the angles α and β to realise this. α is used to get our angle of incidence upon the air pocket close to the critical angle. β is used to get an angle of transmission similar to the ANITA events.

If we wish to get a similar angle of 'reflection' off the ice as in ANITA-III, we need an angle of about 55°. The goal is to lose as little of our signal as possible. We know that most of our signal remains for angles of incidence upon the ice pocket close to the critical angle. From this we can deduce what angle β we need to accomplish this. If we take an angle of incidence of 45° (the critical angle is only a few degrees bigger) we need to solve the following equation

$$n_1 \sin(55 - \beta) = n_2 \sin(45 - \beta), \tag{7.25}$$

which is just Snell's law for our inclined plane. We can find a numerical solution to this: $\sim 18.3°$. This is a somewhat confining angle for β. We can lower this number by allowing a smaller angle of incidence upon the air pocket. The only downside to this, is that we will lose more intensity. Given that we are looking for an angle θ_4, see figure 7.5, of about 55° we can calculate the angle θ_1 to accomplish this. The result of this, as well as the power loss, is shown in figure 7.14. Here we see immediately that for small angles α and β we lose almost all our power. Therefore we are confined to big angles for β for this scenario to explain the ANITA-I

and ANITA-III measurements.[iii].

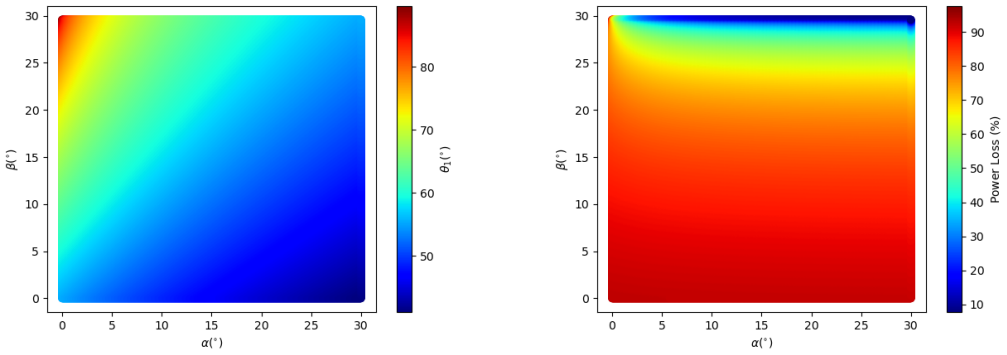

(a) θ_1 such that $\theta_4 = 55°$.

(b) Power loss in %

Figure 7.14: On the left the angle θ_1 is given as a function of α and β, such that $\theta_4 = 55°$. On the right the percentage of power that is lost is given as a function of α and β.

7.4 Inclined Ice and Air Layer

Instead of only varying the inclinations of the ice sheet we could also consider a tilted air pocket under the ice. The choice of which directions the interfaces should be rotated needs some thought. If we wish to look at small arrival angles we can choose angles α and β as in the previous section. At the bottom of the ice we introduce another angles γ, see figure 7.15.

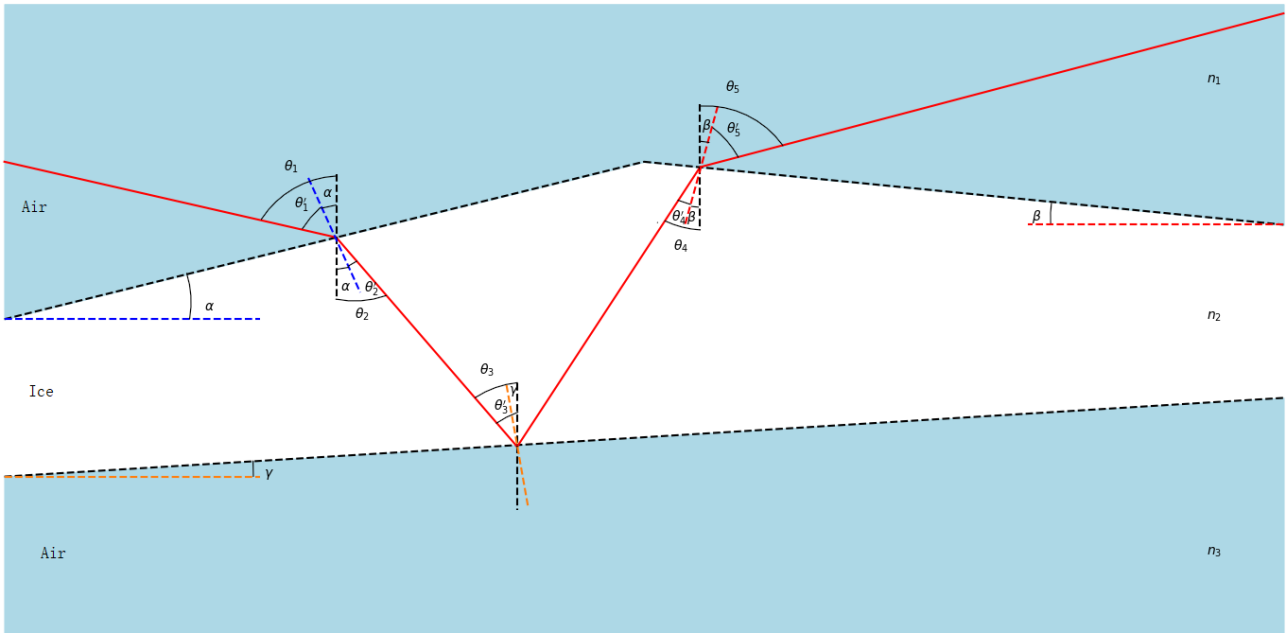

Figure 7.15: Ice sheet with three inclinations and an air pocket beneath.

Some angles can be easily determined from the figure. $\theta_3 = \theta_2$ and $\theta_4 = \theta_3' - \gamma = \theta_2 - 2\gamma$.

[iii] An important note is that this case can explain the ANITA-IV measurements. If α and β are such that we get no TIR, which is only true for small β, there is sufficient power left for the signal to be measured. If β gets bigger or θ_1 gets bigger we get back to the case of TIR which we know can explain ANITA-IV.

Snell's law at each interface determines the angles θ_2 through θ_5 in terms of θ_1

$$\begin{aligned} n_1 \sin(\theta_1 - \alpha) &= n_2 \sin(\theta_2 - \alpha) \\ n_1 \sin(\theta_5 - \beta) &= n_2 \sin(\theta_2 - 2\gamma - \beta). \end{aligned} \tag{7.26}$$

In this scenario we again want TIR at the bottom interface and transmission through the top. This means that θ_3' should exceed the critical angle, while θ_4' is smaller than the critical angle. This leads to two criteria

$$\begin{aligned} \theta_3' &\geq \sin^{-1} \frac{n_3}{n_2} \\ \theta_4' &< \sin^{-1} \frac{n_1}{n_2} \end{aligned} \tag{7.27}$$

Writing this in terms of θ_1 yields

$$\begin{aligned} \sin^{-1}\left(\frac{n_1}{n_2}\sin(\theta_1 - \alpha)\right) + \alpha - \gamma &\geq \sin^{-1}\frac{n_3}{n_2} \\ \sin^{-1}\left(\frac{n_1}{n_2}\sin(\theta_1 - \alpha)\right) + \alpha - 2\gamma - \beta &< \sin^{-1}\frac{n_1}{n_2}. \end{aligned} \tag{7.28}$$

As we have introduced here another variable, without more constraints, the best we can do is find criteria that involve more variables. Solving equations 7.28 for θ_1 results in the following bounds

$$\sin^{-1}\left(\frac{n_2}{n_1}\sin\left(\sin^{-1}\left(\frac{n_1}{n_2}\right) - \alpha + 2\gamma + \beta\right)\right) + \alpha > \theta_1 \geq \sin^{-1}\left(\frac{n_2}{n_1}\sin\left(\sin^{-1}\left(\frac{n_3}{n_2}\right) - \alpha + \gamma\right)\right) + \alpha. \tag{7.29}$$

From this we can find some constraints on the angles for this situation to occur. We know the arcsine is defined if the argument does not exceed 1. From this follows that the upper and lower bound exist if

$$\begin{aligned} \gamma - \alpha &\leq \sin^{-1}\frac{n_2}{n_1} - \sin^{-1}\frac{n_3}{n_2} \\ 2\gamma + \beta &\leq \alpha. \end{aligned} \tag{7.30}$$

If the first of these inequalities is not satisfied, the first criteria of equation 7.28 never holds. If the second is not satisfied, the second criteria of equation 7.28 holds for all $\theta_1 \in [\alpha, 90 + \alpha]$. Lastly we demand the upper bound, if it exists, to be greater than the lower bound. From this follows

$$\gamma + \beta > \sin^{-1}\frac{n_3}{n_2} - \sin^{-1}\frac{n_1}{n_2}. \tag{7.31}$$

All these criteria together give

$$\begin{cases} \gamma - \alpha \leq \sin^{-1}\frac{n_2}{n_1} - \sin^{-1}\frac{n_3}{n_2} & \\ \gamma + \beta > \sin^{-1}\frac{n_3}{n_2} - \sin^{-1}\frac{n_1}{n_2} & \alpha \leq 2\gamma + \beta \\ \sin^{-1}\left(\frac{n_2}{n_1}\sin\left(\sin^{-1}\left(\frac{n_1}{n_2}\right) - \alpha + 2\gamma + \beta\right)\right) + \alpha > \theta_1 & 2\gamma + \beta \leq \alpha \\ \theta_1 \geq \sin^{-1}\left(\frac{n_2}{n_1}\sin\left(\sin^{-1}\left(\frac{n_3}{n_2}\right) - \alpha + \gamma\right)\right) + \alpha & 2\gamma + \beta \leq \alpha \\ 90 + \alpha \geq \theta_1 \geq \sin^{-1}\left(\frac{n_2}{n_1}\sin\left(\sin^{-1}\left(\frac{n_3}{n_2}\right) - \alpha + \gamma\right)\right) + \alpha & 2\gamma + \beta > \alpha \end{cases} \tag{7.32}$$

We can check if this criteria can explain the anomalous ANITA events, by calculating θ_1 for a given θ_5, see figure 7.15, and checking all the criteria. All subsequent figures in this section are 2D representations of 3D data. The full plots are given in appendix D.

Checking the criteria for the ANITA-III measurements, i.e. $\theta_5 = 55°$, and requiring less than 50% intensity loss, results in figure 7.16.

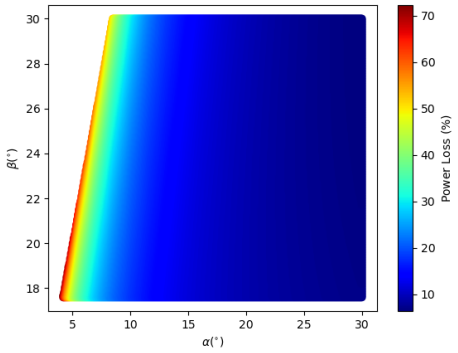

(a) $\gamma = 4°$

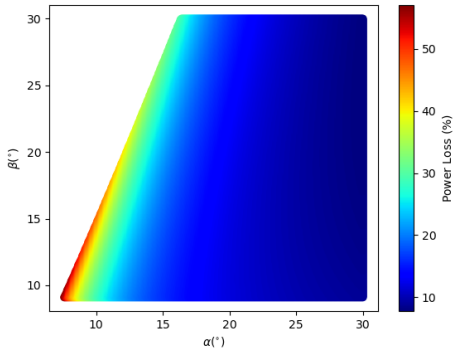

(b) $\gamma = 7°$

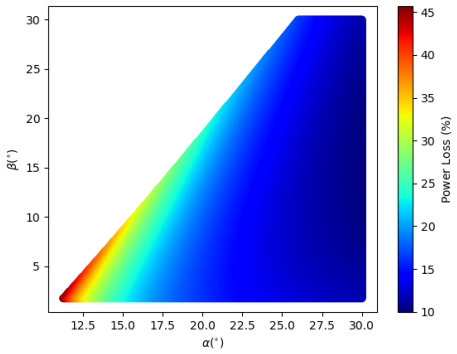

(c) $\gamma = 10°$

Figure 7.16: Power loss of the s polarization as a function of α and β for θ_1 such that $\theta_5 = 55°$, for three values of γ with TIR.

What we see here is that for $\gamma = 4°$, β is restricted to angles greater than $\sim 18°$. As we increase γ, we get the desired result for smaller β, but at the same time we need to increase α.

We can also omit the criteria for TIR, and look at a normal reflection off the air pocket. Doing this results in figure 7.17.

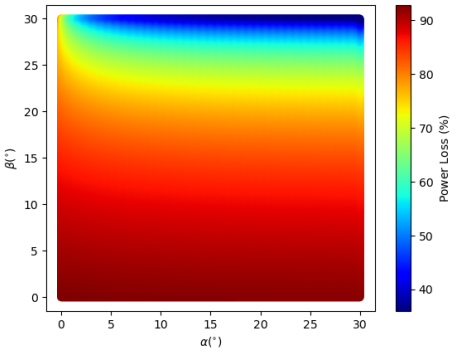

(a) $\gamma = 0°$

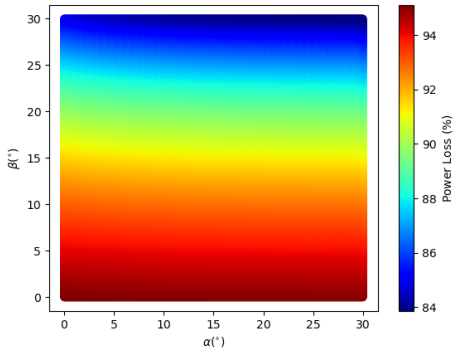

(b) $\gamma = -5°$

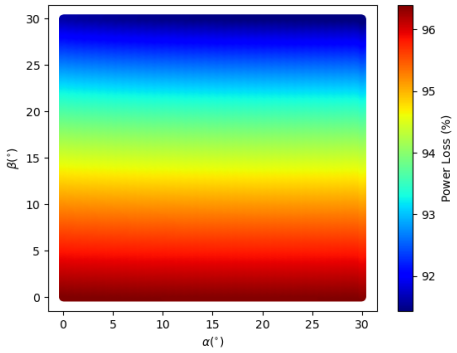

(c) $\gamma = -10°$

Figure 7.17: Power loss of the s polarization as a function of α and β for θ_1 such that $\theta_5 = 55°$, for three values of γ without TIR.

Here we get solutions mainly for negative values of γ, see also appendix D. For $\gamma = 0°$ we get back to figure 7.14b. Lowering γ results in so much power loss that this cannot explain the anomalous ANITA-I and ANITA-III measurements.

Now we can do the same for the ANITA-IV measurements. Checking the power loss for incident angle θ_1 such that $\theta_5 = 84°$ with TIR, results in figure 7.18.

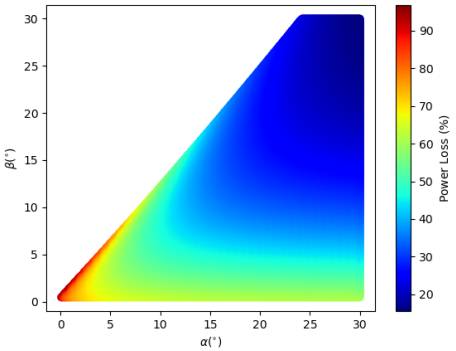

(a) $\gamma = 0°$

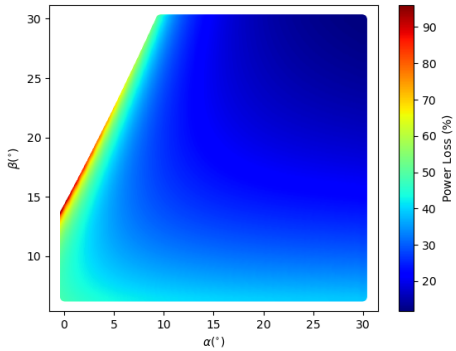

(b) $\gamma = -5°$

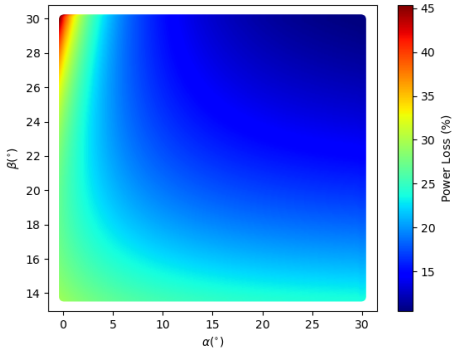

(c) $\gamma = -10°$

Figure 7.18: Power loss of the s polarization as a function of α and β for θ_1 such that $\theta_5 = 84°$, for three values of γ with TIR.

This looks promising. For $\gamma = 0°$ we get back to figure 7.13, which we know provides a solution for relatively small angles α and β. When lowering γ we see that for all angles $0° \leq \alpha \leq 30°$ we lose little power. Only β increases as γ decreases.

Checking the same but without TIR results in figure 7.19.

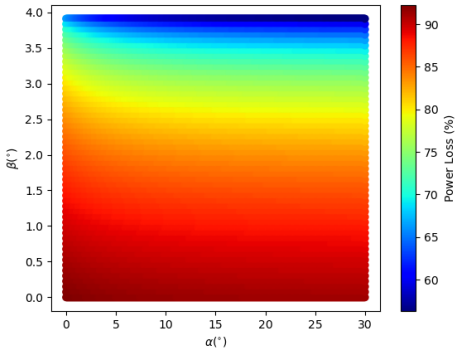

(a) $\gamma = -3°$

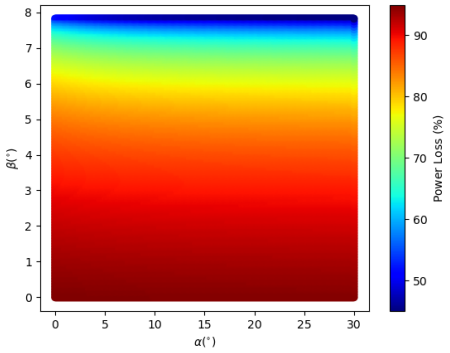

(b) $\gamma = -6°$

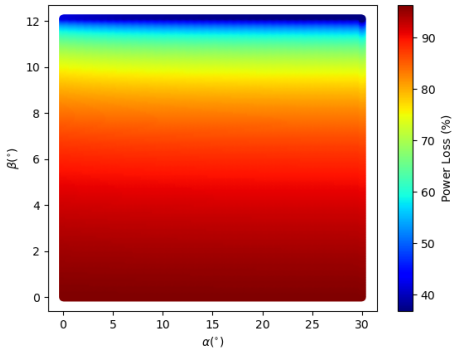

(c) $\gamma = -9°$

Figure 7.19: Power loss of the s polarization as a function of α and β for θ_1 such that $\theta_5 = 84°$, for three values of γ without TIR.

From this it is clear that there is a narrow region for β for a given γ where there is a power loss that does not exceed 50% too much.

All in all does this scenario provide an explanation for all the anomalous ANITA measurements. This requires angles α and/or (depending on the incident angle) β in the order or of $10°$

7.5 Ice and Air Layer With Multiple Inclinations

We could in principle introduce an arbitrary amount of reflections in the ice, each from a surface at a different angle. Even though all odd number of reflections will produce a non inverted signal, multiple number of reflections greatly reduces the intensity of the signal. Not only can we construct unrealistic scenarios with the ice this way, the signal will also probably be too weak to measure.

8 Conclusion and Discussion

The goal of this thesis was to find an explanation to the anomalous ANITA measurements. An explanation was sought in different ice geometries through which a radio signal would propagate. There were a couple of scenarios that looked promising. First was the horizontal layered system with an air layer under the ice. Even though a normal reflection off this air layer produces a non inverted radio signal, there is too much power loss after propagation through the system for the signal to be measured.

Introducing two inclinations in the ice sheet and an air layer below results also in a non inverted radio signal for arrival angles at the antenna of $\sim 84°$, similar to those of ANITA-IV. After propagation almost half the signal's intensity is left. The downside to this situation is that it is restricted to relatively big angles, it therefore can not explain the ANITA-I and ANITA-III events.

Introducing a normal reflection in this system as opposed to TIR, could in principle solve this problem. However, for arrival angles similar to those of ANITA-I and ANITA-III we found that the geometry was confined to relatively big inclinations. It could explain the ANITA-IV events.

Introducing a tilted ice pocket under the ice resulted in a situation which can explain all anomalous events. for small arrival angles, similar to ANITA-I and ANITA-III, this requires a tilt α and β in the order of $10°$. When allowing for a normal reflection we are confined to a narrow band of β values around $30°$ and no tilt of the ice pocket. The ANITA-IV events could be explained by angles $0° \leq \beta_{\text{min}} \leq 14°$ depending on the angle γ. For the case of no TIR there was also a narrow band of allowed β values that increased from $4°$ to $12°$ as γ decreased from $0°$ to $-9°$.

It was found that the dimensions of the structures should be in the order of meters.

If structures like these are ubiquitous in Antarctica, this could provide a possible explanation for the anomalous measurements made during ANITA-I, ANITA-III and ANITA-IV.

An important note is that the layer under the ice is chosen to be air, but this does not need to be the case. The found criteria work for all values of the refractive indices as long as they satisfy all relevant criteria. Therefore, other layers under the ice could be thought of that result in a layer with a smaller refractive index than ice. The choice of air is, because air pockets are known to exist under ice and a refractive index was needed to make explicit calculations.

Appendices

A Curvature of the Earth

To justify the implication of a flat earth we will make a simple calculation. Assuming the Earth is perfectly spherical, we can look at a cross section of the Earth in the (x, z) plane. This gives an equation of a circle with the radius of the earth R_E

$$x^2 + z^2 = R_E^2. \tag{A.1}$$

By implicit differentiation with respect to x of equation A.1, we get

$$2x + 2z\frac{\mathrm{d}z}{\mathrm{d}x} = 0. \tag{A.2}$$

At a distance s from geographic south, see figure A.1, we get to the point $(x, z) = \left(R_E \sin\frac{s}{R_E}, R_E \cos\frac{s}{R_E}\right)$. The derivative at this point is given by equation A.2

$$\frac{\mathrm{d}z}{\mathrm{d}x} = -\tan\frac{s}{R_E} \tag{A.3}$$

For $s = 300km$, which is approximately the horizontal distance traversed by signals from an air shower with zenith angle 80° in the simulation, this corresponds to a rotation from the, assumed flat, horizontal ground, of about 2.5°. As this is a small angle, which for smaller zenith angles will be even smaller, we can ignore the earths curvature.

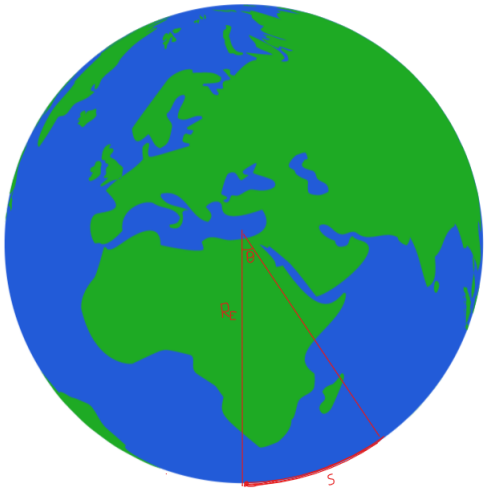

Figure A.1: Distance s from geographic south in the x,z plane.

B Transmission Coefficients

Here it will be shown that the Fresnel coefficients for transmission, equations 4.11 and 4.10, can safely be ignored in the propagation of a signal through the atmosphere. For transmission through an interface we get the situation of figure 5.3. The signal is transmitted from a medium with refractive index $n(h)$ to a medium with refractive index $n(h-d)$. With the refractive index as given by equation 5.1. Substituting in the Fresnel coefficients yield the plots in figure B.1. The coefficients are calculated at a height of $h = 1m$, because the $n(z)$ has the greatest values

close to sea level $z = 0$. From the figure we see that both coefficients are strictly positive and equal to 1 for almost all angles. This means t_s and t_p both don't alter the phase of an incident wave and don't affect the amplitude of the wave. Both of these are therefore ignored in calculations of propagation through air.

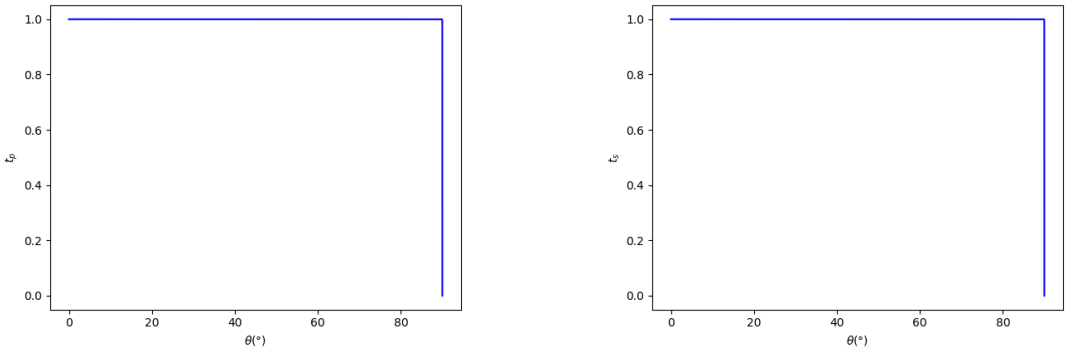

((a)) ((b))

Figure B.1: Transmission coefficients for p polarization (left) and s polarization (right) for transmission from air layer at a height of $h = 1m$ to the next layer $d = 10cm$ lower.

C Phase Delay

We will look at a delta function waveform propagating through a medium of constant refractive index. Let $\mathbf{E}$ be defined as in equation 4.4

$$\mathbf{E}(\mathbf{r}, t) = \frac{\mathbf{E}_0}{2\pi}\delta\left(t - \frac{n}{c}\hat{\mathbf{k}} \cdot \mathbf{r}\right). \tag{C.1}$$

Taking the Fourier transform results in

$$\mathbf{E}(\mathbf{r}, \omega) = \frac{1}{(2\pi)^{\frac{3}{2}}}\mathbf{E}_0 e^{i\frac{n\omega}{c}\hat{\mathbf{k}}\cdot\mathbf{r}}. \tag{C.2}$$

From equation 5.19 we know what happens to the Fourier components after travelling a distance $\Delta\mathbf{r}$ through a medium of refractive index n

$$\mathbf{E}(\mathbf{r} + \Delta\mathbf{r}, \omega) = \frac{1}{(2\pi)^{\frac{3}{2}}}\mathbf{E}_0 e^{i\frac{n\omega}{c}\hat{\mathbf{k}}\cdot\mathbf{r}} e^{i\mathbf{k}\cdot\Delta\mathbf{r}}. \tag{C.3}$$

Now taking the inverse Fourier transform yields the pulse after propagation

$$\begin{aligned}\mathbf{E}(\mathbf{r} + \Delta\mathbf{r}, t) &= \frac{1}{\sqrt{2\pi}}\int_{-\infty}^{\infty}\frac{1}{(2\pi)^{\frac{3}{2}}}\mathbf{E}_0 e^{i\frac{n\omega}{c}\hat{\mathbf{k}}\cdot\mathbf{r}} e^{i\mathbf{k}\cdot\mathbf{r}}\mathrm{d}\omega \\ &= \frac{\mathbf{E}_0}{2\pi}\delta\left(t - \frac{n\omega}{c}\hat{\mathbf{k}} \cdot (\mathbf{r} + \Delta\mathbf{r})\right).\end{aligned} \tag{C.4}$$

This is just the original pulse shifted in time. It is because of this that phase delay is ignored and just time delays are taken into account. Note that we have taken the refractive indices to be the same, this need not be the case. For different refractive indices we would just get two terms in the delta function which again is just a shift in time.

D 3D Depiction of Power Loss as a Function of α, β and γ

Here the 3D data for the power loss as a function of α, β and γ of section 7.4 is given.

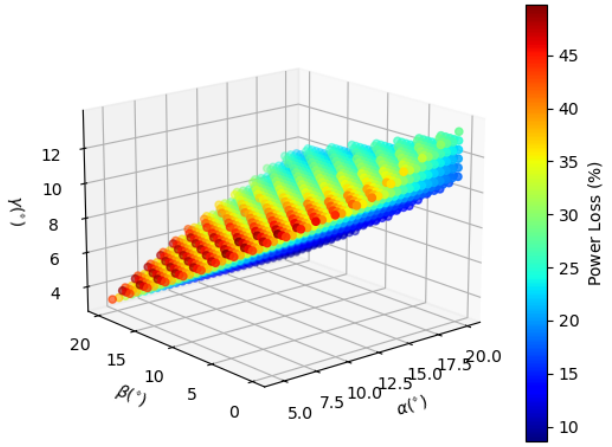

Figure D.1: Power loss for the points (α, β, γ), where θ_1 is such that $\theta_5 = 55°$. With TIR.

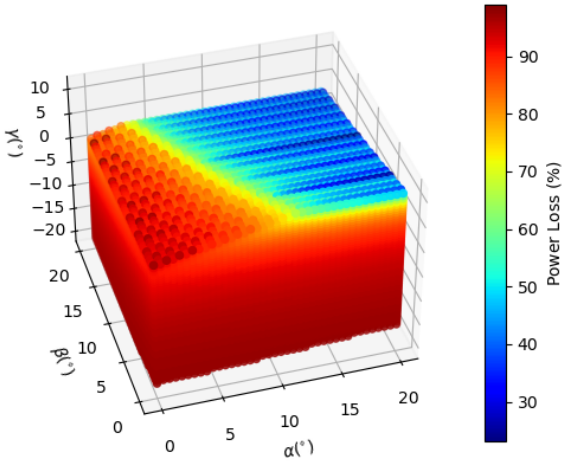

Figure D.2: Power loss for the points (α, β, γ), where θ_1 is such that $\theta_5 = 55°$. Without TIR.

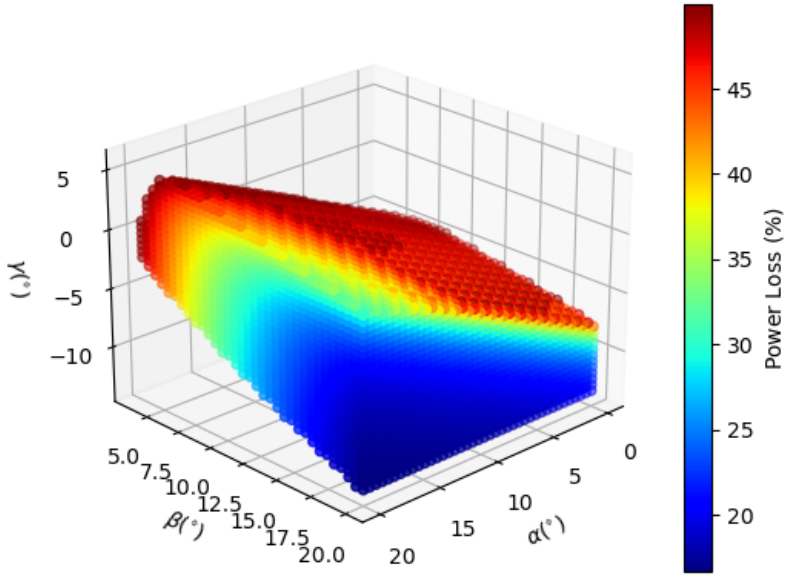

(a)

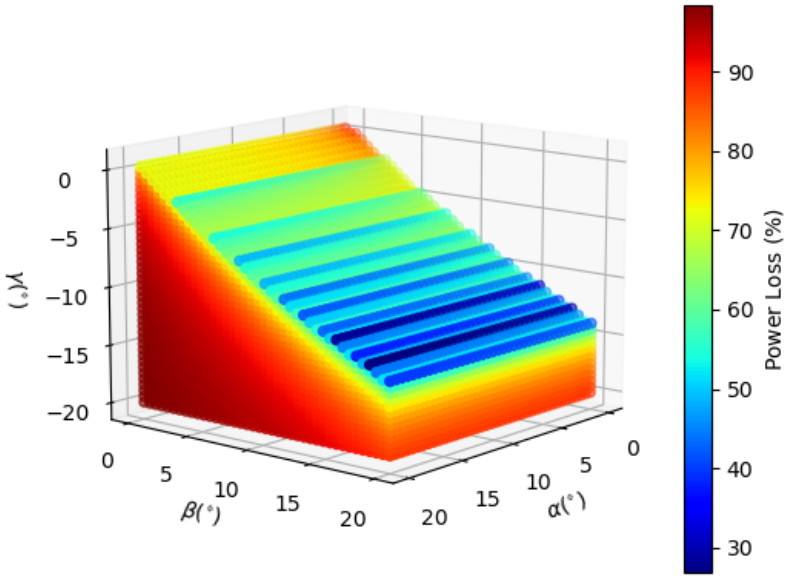

(b)

Figure D.3: Power loss for the points (α, β, γ) and θ_1 such that $\theta_5 = 84°$. On the top with TIR and on the bottom without TIR.

E Python Code

The python code of the simulation can be found at `https://gitlab.science.ru.nl/astroparticle/student-projects/colin-saba-bsc`.

References

[1] S. Jansen. *Radio for the Masses: Cosmic ray mass composition measurements in the radio frequency domain*. https://hdl.handle.net/2066/155739, 2016.

[2] Michael Zeilik and Stephen A. Gregory. *Introductory astronomy astrophysics*. 4. ed., [Nachdr.] Singapore [u.a.]: Brooks/Cole Thomson Learning, 2007. Getr. Zählung. ISBN: 9780030062285.

[3] David Griffiths. *Introduction to elementary particles*. 2008. ISBN: 978-3-527-40601-2.

[4] Karl-Heinz Kampert and Alan A. Watson. "Extensive air showers and ultra high-energy cosmic rays: a historical review". In: *The European Physical Journal H* 37.3 (July 2012), pp. 359–412. DOI: 10.1140/epjh/e2012-30013-x. URL: https://doi.org/10.1140%5C%2Fepjh%5C%2Fe2012-30013-x.

[5] Jaime Alvarez-Muñiz et al. "Radio pulses from ultra-high energy atmospheric showers as the superposition of Askaryan and geomagnetic mechanisms". In: *Astroparticle Physics* 59 (July 2014), pp. 29–38. DOI: 10.1016/j.astropartphys.2014.04.004. URL: https://doi.org/10.1016%5C%2Fj.astropartphys.2014.04.004.

[6] P.W. Gorham et al. "The Antarctic Impulsive Transient Antenna ultra-high energy neutrino detector: Design, performance, and sensitivity for the 2006–2007 balloon flight". In: *Astroparticle Physics* 32.1 (Aug. 2009), pp. 10–41. DOI: 10.1016/j.astropartphys.2009.05.003. URL: https://doi.org/10.1016%2Fj.astropartphys.2009.05.003.

[7] A. Romero-Wolf et al. "Observation of ultra-high-energy cosmic rays with the ANITA balloon-borne radio interferometer". In: *Nuclear Instruments and Methods in Physics Research Section A: Accelerators, Spectrometers, Detectors and Associated Equipment* (2010). ISSN: 0168-9002. DOI: https://doi.org/10.1016/j.nima.2010.11.136. URL: https://www.sciencedirect.com/science/article/pii/S0168900210026835.

[8] P. W. Gorham et al. "Observation of an Unusual Upward-Going Cosmic-Ray-like Event in the Third Flight of ANITA". In: *Physical Review Letters* 121.16 (Oct. 2018). DOI: 10.1103/physrevlett.121.161102. URL: https://doi.org/10.1103%5C%2Fphysrevlett.121.161102.

[9] P. W. Gorham et al. "Unusual Near-Horizon Cosmic-Ray-like Events Observed by ANITA-IV". In: *Physical Review Letters* 126.7 (Feb. 2021). DOI: 10.1103/physrevlett.126.071103. URL: https://doi.org/10.1103%2Fphysrevlett.126.071103.

[10] Jack H. Collins, P. S. Bhupal Dev, and Yicong Sui. "R-Parity Violating Supersymmetric Explanation of the Anomalous Events at ANITA". In: *Physical Review D* 99.4 (Feb. 2019). DOI: 10.1103/physrevd.99.043009. URL: https://doi.org/10.1103%5C%2Fphysrevd.99.043009.

[11] J. Peatross & M. Ware. *Physics of Lights and Optics*. 2015. URL: https://optics.byu.edu/textbook.

[12] David J Griffiths. *Introduction to electrodynamics*. Pearson, 2013.

[13] Brian F. Hanley. "A practical method for estimating specific refractive index increments for flexible non-electrolyte polymers and copolymers in pure and mixed solvents using the Gladstone-Dale and Lorentz-Lorenz equations in conjunction with molar refraction structural constants, and solvent physical property databases". In: *Materials Today Communications* 25 (2020), p. 101644. ISSN: 2352-4928. DOI: https://doi.org/10.1016/j.mtcomm.2020.101644. URL: https://www.sciencedirect.com/science/article/pii/S2352492820326556.

[14] E. Hecht. *Optics, 5e*. Addison-Wesley, 2002. ISBN: 9789353942595. URL: https://books.google.nl/books?id=BhDCDwAAQBAJ.

[15] Wikimedia Commons. *File:Superior and inferior mirage.svg — Wikimedia Commons, the free media repository*. [Online; accessed 18-January-2023]. 2022. URL: https://commons.wikimedia.org/w/index.php?title=File:Superior_and_inferior_mirage.svg&oldid=695947184.

[16] Jaime Alvarez-Muñiz et al. "Simulations of reflected radio signals from cosmic ray induced air showers". In: *Astroparticle Physics* 66 (2015), pp. 31–38. ISSN: 0927-6505. DOI: https://doi.org/10.1016/j.astropartphys.2014.12.005. URL: https://www.sciencedirect.com/science/article/pii/S0927650514001911.

[17] Antonio Rius et al. "Feasibility of GNSS-R Ice Sheet Altimetry in Greenland Using TDS-1". In: 9 (), p. 742. ISSN: 2072-4292. DOI: 10.3390/rs9070742.